Monthly Notices of the ROYAL ASTRONOMICAL SOCIETY

MNRAS **469,** 2886–2906 (2017) doi:10.1093/mnras/stx860

Discovery of giant radio galaxies from NVSS: radio and infrared properties

Pratik Dabhade,[1,5]★ Madhuri Gaikwad,[2] Joydeep Bagchi,[1]★ M. Pandey-Pommier,[3] Shishir Sankhyayan[4] and Somak Raychaudhury[1]

[1]*Inter University Centre for Astronomy and Astrophysics (IUCAA), Pune University Campus, Pune 411007, India*
[2]*National Centre for Radio Astrophysics, TIFR, Post Bag 3, Ganeshkhind, Pune 411007, India*
[3]*University Lyon 1, Ens de Lyon, CNRS, Centre de Recherche Astrophysique de Lyon UMR5574, France*
[4]*Indian Institute of Science Education and Research, Pune 411008, India*
[5]*Leiden Observatory, Leiden University, Niels Bohrweg 2, NL-2333 CA, Leiden, Netherlands*

Accepted 2017 April 5. Received 2017 March 30; in original form 2016 April 14

ABSTRACT

Giant radio galaxies (GRGs) are one of the largest astrophysical sources in the Universe with an overall projected linear size of ∼0.7 Mpc or more. The last six decades of radio astronomy research has led to the detection of thousands of radio galaxies. However, only ∼300 of them can be classified as GRGs. The reasons behind their large size and rarity are unknown. We carried out a systematic search for these radio giants and found a large sample of GRGs. In this paper, we report the discovery of 25 GRGs from the National Radio Astronomy Observatory Very Large Array Sky Survey, in the red-shift range $z \sim 0.07$ to 0.67. Their physical sizes range from ∼0.8 Mpc to ∼4 Mpc. Eight of these GRGs have sizes ≥2 Mpc, which is a rarity. Here, for the first time, we investigate the mid-infrared (IR) properties of the optical hosts of the GRGs and classify them securely into various active galactic nuclei types using the *WISE* mid-IR colours. Using radio and IR data, four of the hosts of the GRGs were observed to be radio-loud quasars that extend up to 2 Mpc in radio size. These GRGs missed detection in earlier searches possibly because of their highly diffuse nature, low surface brightness and lack of optical data. The new GRGs are a significant addition to the existing sample. They will contribute to a better understanding of the physical properties of radio giants.

Key words: galaxies: active – intergalactic medium – galaxies: jets – galaxies: nuclei – quasars: supermassive black holes – infrared: galaxies.

1 INTRODUCTION

Giant radio galaxies (GRGs) represent an extreme class of active galaxies with linear sizes from ∼0.7 to 5 Mpc, thus placing them amongst the largest single astrophysical objects known to us. The first GRG, 3C236, discovered about 40 years ago by Willis, Strom & Wilson (1974), is ∼4.62 Mpc in size and still ranks among the largest known GRGs. Since then only a few other GRGs have been reported. The largest known GRG to date is J1420−0545, which spans 4.95 Mpc (Machalski et al. 2008). Despite various studies on GRGs, no unified model has emerged that can explain the immense physical scale and other physical properties of this extreme class of radio sources. With the advent of large-area sky surveys, like the National Radio Astronomy Observatory (NRAO) Very Large Array (VLA) Sky Survey (NVSS) (Condon et al. 1998), Westerbork Northern Sky Survey (Rengelink et al. 1997) and Sydney University Molonglo Sky Survey (SUMSS) (Mauch et al. 2003), several more GRGs have been found and many more await discovery through dedicated searches.

Morphologically, most of the GRGs show bright hot spots at the end of their radio lobes and are, hence, classified as edge-brightened Fanaroff–Riley class II (FR-II) objects (Fanaroff & Riley 1974). These radio sources are born in the active nuclei at the galactic centre. It is believed that their so-called central engine is a mass-accreting super massive black hole (SMBH) of mass 10^8–10^{10} $M_\odot$, which is responsible for the ejection of the collimated, bipolar relativistic jets orthogonal to an accretion disc (Lynden-Bell 1969; Begelman, Blandford & Rees 1984). In common with normal radio galaxies, GRGs are usually hosted by bright elliptical galaxies. However, recently two extremely massive and fast rotating spiral galaxies have been found that host relativistic jets and lobes that extend to megaparsec scales (Hota et al. 2011; Bagchi et al. 2014), which is exceedingly rare. These extraordinary objects demonstrate that given the right conditions, the central engine of spiral galaxies can launch megaparsec-scale radio jets and form lobes around them.

★ E-mail: pratikdabhade13@gmail.com (PD); joydeep@iucaa.in (JB)

Since the inception of radio astronomy, thousands of radio galaxies (RGs) have been discovered, but only a tiny fraction of them (∼300 so far) are GRGs (Subrahmanyan, Saripalli & Hunstead 1996; Ishwara-Chandra & Saikia 1999; Lara et al. 2001; Schoenmakers et al. 2001; Machalski, Jamrozy & Zola 2001; Saripalli et al. 2005; Machalski et al. 2006; Machalski, Koziel-Wierzbowska & Jamrozy 2007; Kuźmicz & Jamrozy 2012). Of these, only GRGs have been studied in sufficient detail in multiple wavebands to achieve a good understanding of their unusual nature. This puts a restriction on carrying out any statistical study of their properties. Understanding their birth and evolution, the duty cycle of radio activity and the influence of the surrounding intergalactic medium (IGM), which confines the lobes far away from the host galaxy and provides a working surface for the jets to act, are among the most important problems in this field. Since the GRGs are known to extend to large sizes, they are believed to be the last stop of RG evolution. Hence, their study may help us impose important constraints on the various evolutionary models of RGs. For the existence of radio lobes and hot spots at large distances from the active galactic nucleus (AGN), a low-density ambient IGM is implied in which the lobes expand and eventually diffuse out at the end of their lives. It was shown by Safouris et al. (2009) that GRGs can serve as outstanding probes of the IGM via the relation between the morphology of a RG and the properties of the surrounding material, which is part of the large-scale cosmic web. GRGs can also transport enriched material from the host galaxy to large distances and pollute the IGM with non-thermal particles and magnetic fields (Kronberg 1994). This non-thermal magnetized plasma may lurk in the IGM for billions of years, and become a promising source for injecting high-energy seed particles into the turbulent intra-cluster medium and into energetic shock waves associated with megaparsec-scale central radio haloes and peripheral radio relics, which are observed in some merging galaxy clusters (Enßlin & Gopal-Krishna 2001; Bagchi et al. 2006; van Weeren et al. 2010). Thus, GRGs may also play an important role in the high-energy processes related to large-scale structure formation in the Universe.

Despite many observations and various theoretical models proposed, the mechanisms by which the relativistic jets are launched from the accretion discs around massive black holes in AGNs are very poorly understood (Blandford & Znajek 1977; Blandford & Payne 1982). To date, few theoretical models have been proposed to explain the growth of GRGs to such enormous sizes. One of the common explanations for their gigantic size is attributed to the less dense IGM around them, which allows them to expand and grow unhindered (Jamrozy et al. 2008; Subrahmanyan et al. 2008; Safouris et al. 2009; Malarecki et al. 2015). This implies that GRGs are preferentially born in sparser galactic environments. Another theory proposes that GRGs are very old RGs (Kaiser, Dennett-Thorpe & Alexander 1997) that have grown to their current sizes over long time-scales. Detailed multifrequency studies of a larger sample of GRGs is required to validate or challenge these models in addition to discovering more GRGs in diverse galactic environments.

It is also interesting to note that megaparsec-scale radio-emitting plasma lobes of GRGs are the largest known natural reservoirs of magnetic field and non-thermal relativistic particles associated with a single galactic system. This makes GRGs excellent calorimeters for measuring the energy output of the central black holes, because the giant radio lobes are believed to store most of the released energy of black holes for a very long time and they may also reveal multiple radio episodes of black hole activity (Kronberg et al. 2001). Moreover, because the extended lobes of GRGs can contain charged particles long enough for them to be accelerated to extremely high energies (Hillas 1984), it has been suggested (Kronberg 2004; Hardcastle et al. 2009) that shocks within the energetic jets and radio lobes of GRGs are possible sites for the acceleration of ultra-high-energy cosmic rays whose origin is still unknown and a subject of worldwide research (Hörandel 2008; Bauleo & Rodríguez Martino 2009; Hooper 2016).

In this paper, we present a new sample of GRGs, of linear sizes in the range 0.8 Mpc to 3.7 Mpc, which were discovered during our extensive search of the 1.4-GHz radio images available in the NVSS. In the forthcoming papers, we will present more samples of GRGs along with the results of a statistical analysis and multiwavelength studies of their properties. The paper is organized as follows. In Section 2, we present the optical, radio and near-infrared (IR) analysis of the GRG sample along with an estimation of the mass of the central black hole in the AGN. In Section 3, we discuss the individual GRGs and their physical properties. In Section 4, we describe their collective properties and discuss important results and their wider astrophysical implications. Finally, in Section 5, we summarize our work and discuss the future possibilities. Throughout the paper, we adopt the flat ΛCDM cosmological model based on the latest Planck results ($H_o = 67.8$ km s^{-1} Mpc^{-1}, $\Omega_m = 0.308$) (Planck Collaboration XIII 2016). We use it to determine the linear sizes, luminosities and other relevant physical parameters of the GRGs. The Ned Wright cosmology calculator (Wright 2006) was used to obtain parameters like comoving distance (D_c), luminosity distance (D_L) and scale (kpc arcsec^{-1}).

2 MULTIFREQUENCY PROPERTIES OF GRG SAMPLE

In Table 1, we report the multifrequency properties of our GRG sample. Henceforth, the GRGs are identified with labels GRG1, GRG2, GRG3, etc. Eight of the reported 25 GRGs have projected linear size ≥2 Mpc with the largest extending to ∼3.7 Mpc, which places them among the largest RGs known so far. Basic information, like sky position of the optical host galaxy (RA and Dec.), red shift, angular size (arcminutes), physical size (Mpc), radio flux density $S_{i(1.4\,\mathrm{GHz})}$ and power, is tabulated in Table 1. The angular size of the GRGs was estimated using the available radio maps. The angular extent was taken to be the separation between the peaks (radio brightness) of the outermost lobe components. Only sources with angular size ≥3 arcmin were selected. The linear projected sizes of the GRGs in Table 1 were then computed using (Kellermann & Verschuur 1988)

$$d = \frac{\theta \times D_c}{(1+z)} \times \frac{\pi}{10\,800} \quad (1)$$

where θ is the angle subtended by the source in the sky (arcminutes), z is the red shift, D_c is the comoving distance (Mpc) and d is the projected linear size of the source (Mpc).

2.1 Identification of new GRGs and radio analysis

All of the 25 new GRGs were discovered in the 1.4-GHz NVSS images via an extensive search for large-scale double radio sources. This was done manually by careful visual inspection of NVSS radio maps. A search for more GRGs from NVSS is being carried out under our project *SAGAN*.[1] SAGAN stands for Search and Analysis

[1] https://sites.google.com/site/anantasakyatta/sagan

Table 1. Basic GRG information: z† indicates spectroscopic red shifts. The linear projected size (Mpc) is computed using equation (1). $S_{i(1.4\,\mathrm{GHz})}$ is the integrated flux of the source. $P_{1.4\,\mathrm{GHz}}$ is the radio power computed using equation (2).

ID	RA (J2000)	Dec. (J2000)	Angular size (arcmin)	z	Linear size (Mpc)	$S_{i(1.4\,\mathrm{GHz})}$ (mJy)	$P_{1.4\,\mathrm{GHz}}$ (10^{25} W Hz^{-1})
GRG1	00:16:04.3	+04:20:24.1	6.9	0.43281 ± 0.00009†	2.40	50 ± 5	1.7 ± 0.2
GRG2	00:22:24.9	−08:18:45.7	6.2	0.57147 ± 0.00011†	2.50	259 ± 24	14.6 ± 1.3
GRG3	03:15:36.2	−07:43:38.8	3.3	0.269 ± 0.033	0.86	151 ± 16	2.2 ± 0.2
GRG4	04:29:25.8	+00:33:04.8	6.6	0.468 ± 0.092	2.40	111 ± 10	4.5 ± 0.7
GRG5	04:49:32.3	−30:26:37.8	7.5	0.31496 ± 0.00015†	2.14	94 ± 9	1.8 ± 0.2
GRG6	08:02:48.8	+49:27:23.8	4.3	0.678 ± 0.053	1.88	52 ± 7	3.9 ± 0.5
GRG7	08:57:01.7	+01:31:30.9	6.2	0.27336 ± 0.00007†	1.58	99 ± 9	1.5 ± 0.1
GRG8	10:58:38.6	+24:45:35.1	10.4	0.201 ± 0.016	2.13	147 ± 12	1.3 ± 0.1
GRG9	10:59:20.1	−17:09:20.8	11.5	0.1027 ± 0.0005†	1.33	154 ± 7	0.4 ± 0.01
GRG10	13:27:41.3	+57:49:43.4	12.1	0.12018 ± 0.00001†	1.61	89 ± 4	0.3 ± 0.009
GRG11	13:27:43.5	+17:48:37.3	3.1	0.65688 ± 0.00025†	1.33	70 ± 12	4.9 ± 0.8
GRG12	20:08:43.3	+00:49:18.9	11	0.412 ± 0.094	3.71	81 ± 3	2.6 ± 0.4
GRG13	20:34:49.2	−26:30:36.4	6.7	0.10329 ± 0.00015†	0.78	76 ± 6	0.2 ± 0.01
GRG14	20:59:39.8	+24:34:23.9	8.2	0.116 ± 0.019	1.06	149 ± 8	0.4 ± 0.02
GRG15	22:33:01.3	+13:15:02.5	16	0.093 ± 0.011	1.71	125 ± 4	0.24 ± 0.008
GRG16	22:50:39.1	+28:44:45.5	8.4	0.097 ± 0.009	0.93	120 ± 9	0.2 ± 0.01
GRG17	22:56:15.1	−36:17:59.1	14.5	0.090252 ± 0.00015†	1.51	195 ± 11	0.3 ± 0.02
GRG18	23:04:44.8	−10:50:48.2	4.3	0.21026 ± 0.00018†	0.91	58 ± 8	0.5 ± 0.07
GRG19	23:12:01.3	+13:56:55.9	11.4	0.14041 ± 0.00001†	1.74	338 ± 26	1.4 ± 0.1
GRG20	23:16:20.1	−01:02:07.3	6.8	0.221 ± 0.029	1.50	90 ± 5	0.9 ± 0.07
GRG21	23:26:23.2	+24:58:40.4	11.7	0.25497 ± 0.00002†	2.88	274 ± 27	3.6 ± 0.3
GRG22	23:28:49.9	−08:25:12.7	4.7	0.555 ± 0.056	1.87	63 ± 7	3.4 ± 0.3
GRG23	23:35:52.1	+52:15:39.9	10.2	0.070649 ± 0.00015†	0.85	95 ± 8	0.10 ± 0.008
GRG24	23:49:29.7	−00:03:05.8	4.3	0.187 ± 0.049	0.84	28 ± 3	0.20 ± 0.02
GRG25	23:55:31.6	+02:56:07.1	8.1	0.657 ± 0.235	3.48	80 ± 9	5.7 ± 1.7

of GRGs with Associated Nuclei. In this project, for the first time, we aim to make a sample of all known GRGs and find new GRGs from the existing survey data. Our search has yielded more than 150 new giant RG candidates and we present only those confirmed as a GRG in this paper. The criteria to form the sample of 25 GRGs reported in this paper are:

(i) Double radio sources with angular size ≥3 arcmin.
(ii) The coincidence of the radio core and the host galaxy (as seen optically) confirmed by overlaying radio and optical maps.
(iii) Availability of reliable red-shift (spectroscopic or photometric) information of the host galaxy from various optical surveys.

Recently, similar work with different methods was carried out by Proctor (2016). The author identified radio sources ≥4 arcmin as giant radio source candidates via automated pattern recognition algorithms. Information such as host galaxy identification and red shift, which is imperative for confirming the actual giant radio nature of a galaxy, is not supplemented in Proctor (2016).

NVSS is a 1.4-GHz continuum survey covering the entire sky north of −40° declination (Condon et al. 1998). NVSS images are made with a relatively large restoring beam (45 arcsec full width at half-maximum or FWHM) to yield the high surface-brightness sensitivity needed for completeness and photometric accuracy. Their rms brightness fluctuations are about 0.45 mJy beam^{-1} = 0.14 K (Stokes I) and 0.29 mJy beam^{-1} = 0.09 K (Stokes Q and U). The rms uncertainties in right ascension and declination vary from <1 arcsec for relatively strong (S > 15 mJy) point sources to 7 arcsec for the faintest (S = 2.3 mJy) detectable sources. The completeness limit is about 2.5 mJy.

For a more detailed morphology of the GRGs and identification of the AGN core, VLA high-resolution FIRST (Faint Images of the Radio Sky at 20 cm) (Becker, White & Helfand 1995) survey data were employed. The FIRST survey at 1.4 GHz was done using the NRAO VLA in its B configuration, using 2 × 7 3-MHz frequency channels centred at 1365 and 1435 MHz. FIRST survey maps have 1.8 arcsec pixels, a restoring beam of 5 arcsec and a typical rms of 0.15 mJy. FIRST data for GRG2, GRG3, GRG7, GRG8, GRG9, GRG20, GRG22, GRG24 and GRG25 are available. In addition, we searched the SUMSS data and obtained the flux density of a few GRGs at 843 MHz. SUMSS is an imaging survey (Mauch et al. 2003) of the sky south of declination $\delta = -30^\circ$ at 843 MHz. The survey has a resolution of $45 \times 45 cosec|\delta|$ arcsec^2. SUMSS is similar in sensitivity and resolution to the northern NVSS. The SUMSS data are available only for GRG5 and GRG17, and they provide their flux density at 843 MHz.

The integrated flux densities (S_i) of GRGs were computed using NVSS maps in Common Astronomy Software Applications (CASA) using the task CASA-VIEWER. The radio colour maps overlaid with contours for GRGs shown in Fig. 1 were produced using the NVSS images. For this purpose, the *Cubehelix* colour scheme was used to make colour maps using task CASA-VIEWER in CASA. The *Cubehelix* colour scheme gives more weight to green and yellow, which the human eye is more sensitive to, thereby bringing out essential details in the radio images better (Green 2011).

Radio powers for GRGs were calculated using (Donoso, Best & Kauffmann 2009)

$$P_{1.4} = 4\pi D_L^2 S_{1.4} (1+z)^{\alpha-1} \quad (2)$$

where D_L is the luminosity distance, $S_{1.4}$ is the measured radio flux at 1.4 GHz, $(1+z)^{\alpha-1}$ is the standard k-correction used in radio astronomy and α is the radio spectral index ($S_\nu \propto \nu^{-\alpha}$), for which we adopt a universal value of −1, which is usually observed for RGs. This value of α also takes care of the steepness for some sources.

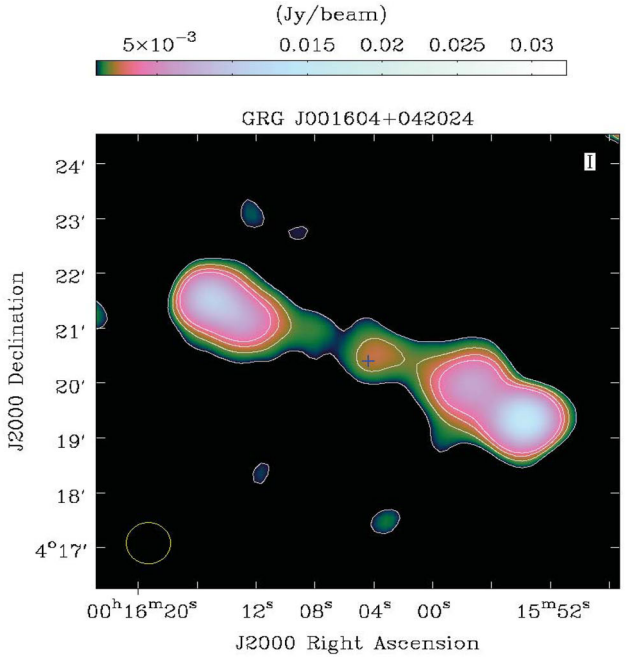

(a) **GRG1 (Linear size = 2.40 Mpc)**

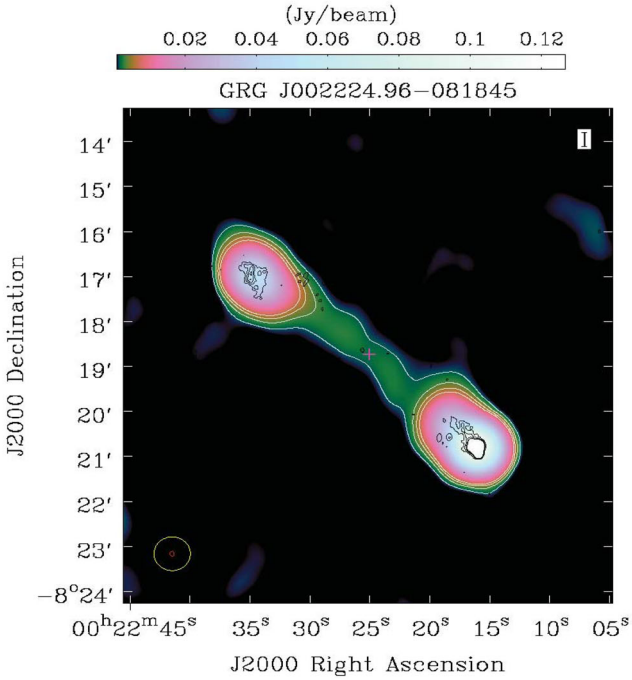

(b) **GRG2 (Linear size = 2.50 Mpc)**

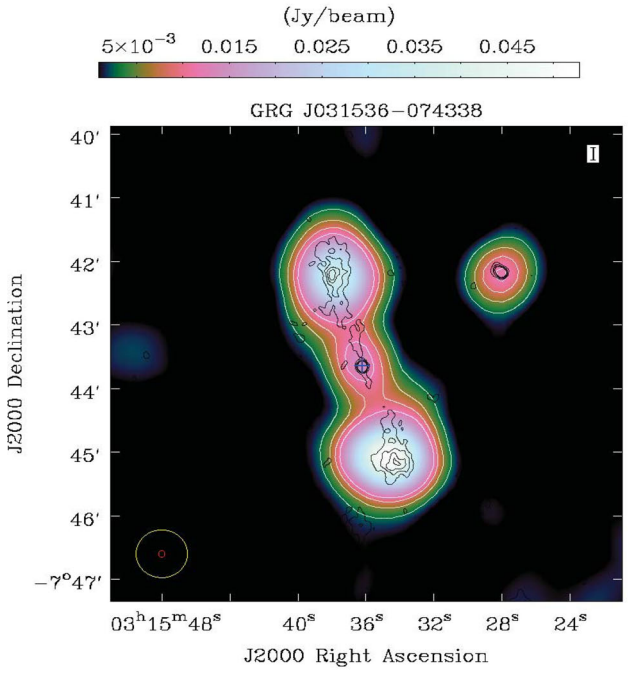

(c) **GRG3 (Linear size = 0.86 Mpc)**

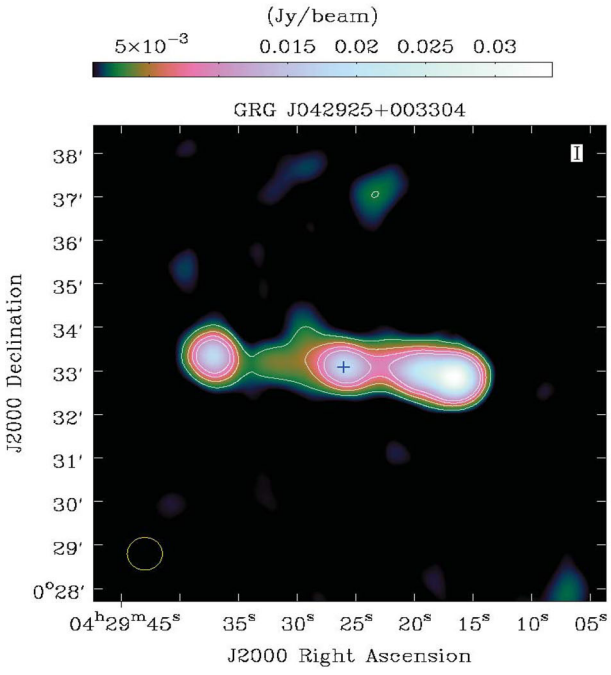

(d) **GRG4 (Linear size = 2.40 Mpc)**

Figure 1. NVSS colour (Cubehelix) and contour maps of GRG1 to GRG25 made using task VIEWER in CASA with relative contour levels as [0.2, 0.4, 0.6, 0.8] mJy beam^{-1}. The beam size for NVSS is represented in yellow (45 × 45 arcsec FWHM) and for FIRST in red (5 × 5 arcsec FWHM) at the bottom left corner of each image. The white contours are for NVSS and the black contours (relative contour levels as [0.2, 0.4, 0.6, 0.8] mJy beam^{-1}) are for the FIRST survey. The (optical) position of the host galaxy is marked with a + symbol.

2.2 Optical analysis

The central regions of the GRGs were searched in the optical band for host galaxies. The brightest galaxy within 1 arcmin of the central peak was identified as a host galaxy. In many cases, the host galaxies overlap with the compact radio cores detected in NVSS and in some cases in the VLA FIRST survey. For optical images and spectroscopic red shifts, we used the Sloan Digital Sky Survey (SDSS) (York et al. 2000), a major multi-filter imaging and

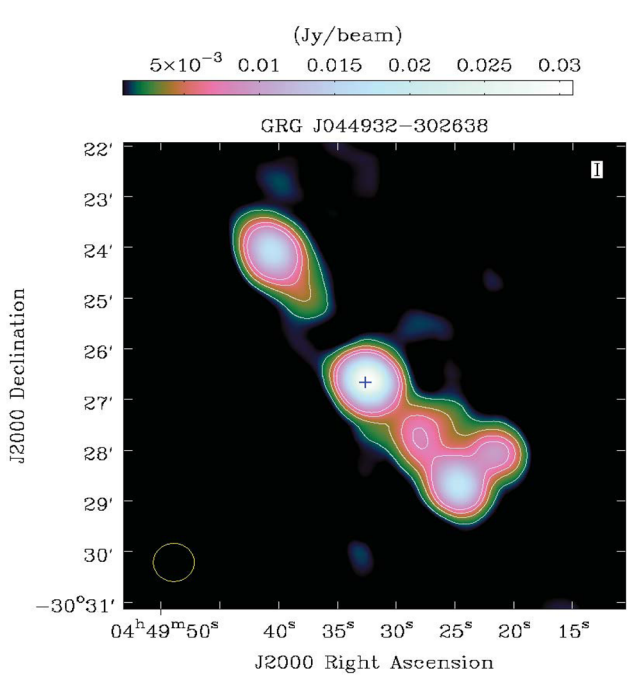

(e) **GRG5 (Linear size = 2.14 Mpc)**

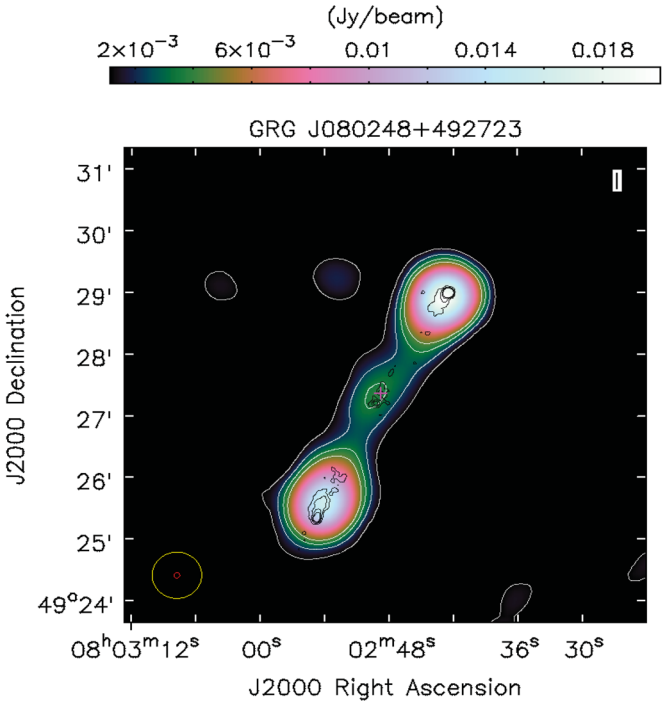

(f) **GRG6 (Linear size = 1.88 Mpc)**

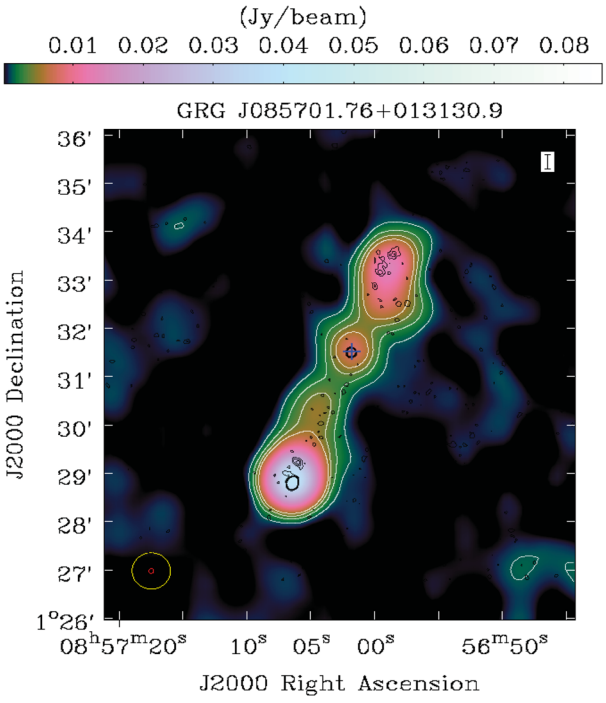

(g) **GRG7 (Linear size = 1.58 Mpc)**

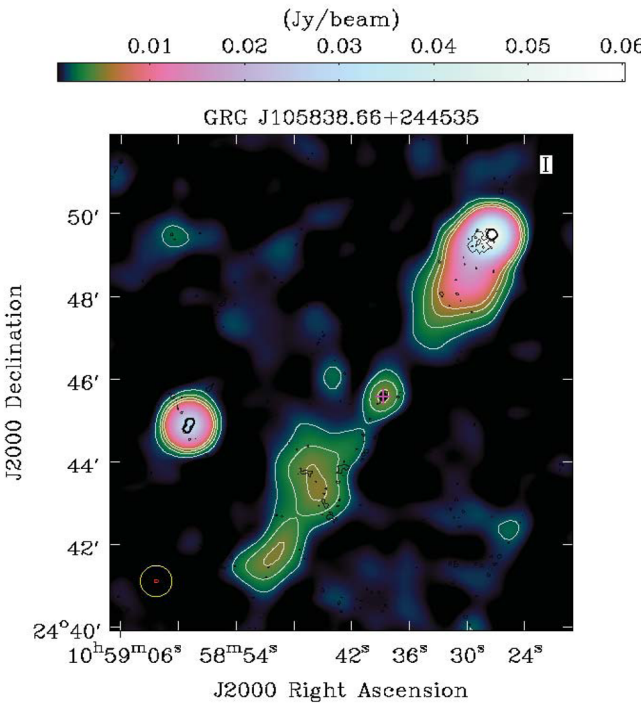

(h) **GRG8 (Linear size = 2.13 Mpc)**

Figure 1 – *Continued*

spectroscopic red-shift survey using a dedicated 2.5-m wide-angle optical telescope at Apache Point Observatory. SDSS Data Release 12 (DR12) is the final data release of SDSS-III, containing all SDSS observations to 2014 July. SDSS also provides CCD images in five filters (u, g, r, i and z) and estimated photometric red shifts (photoZ), which were used if spectroscopic red shifts were unavailable. The photoZ red shifts are quoted for the host galaxies of GRG3, GRG4, GRG6, GRG8, GRG12, GRG14, GRG15, GRG16, GRG20, GRG22, GRG24 and GRG25. SDSS optical colour images of the host galaxies are shown in Fig. A2. The spectroscopic red shifts of GRG1, GRG2, GRG7, GRG10, GRG11, GRG19 and GRG21 were obtained from SDSS DR12 (Alam et al. 2015). Host galaxies with

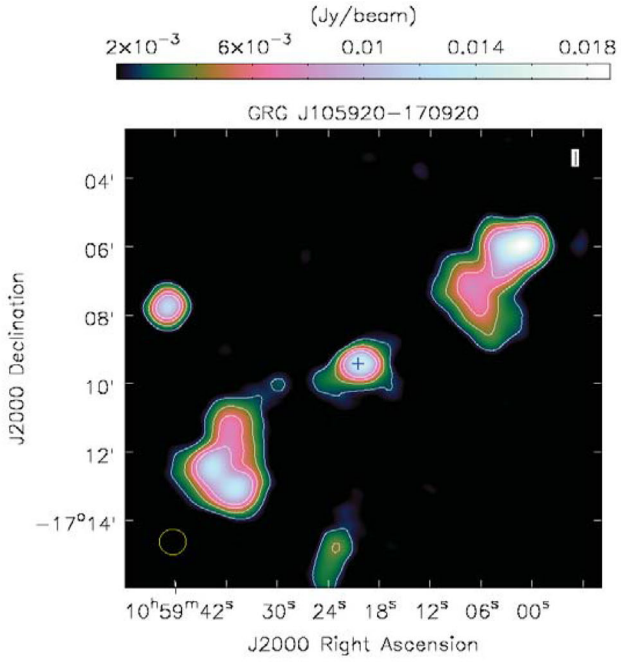

(i) **GRG9 (Linear size = 1.33 Mpc)**

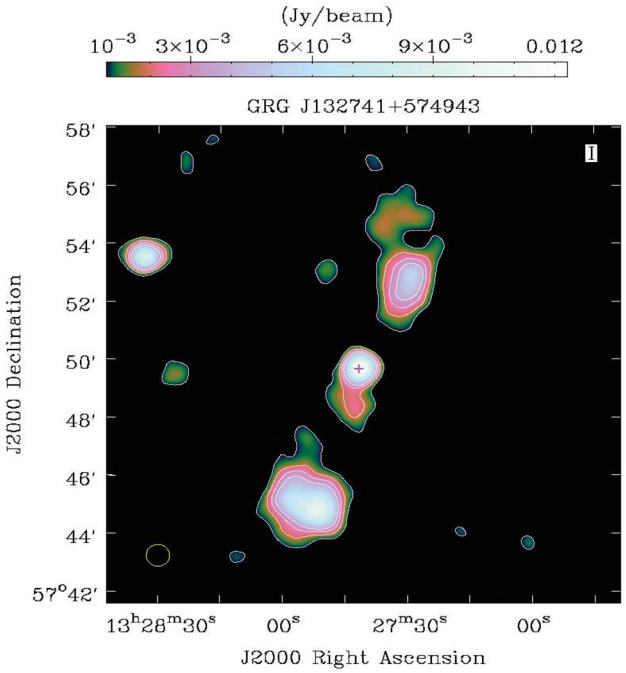

(j) **GRG10 (Linear size = 1.61 Mpc)**

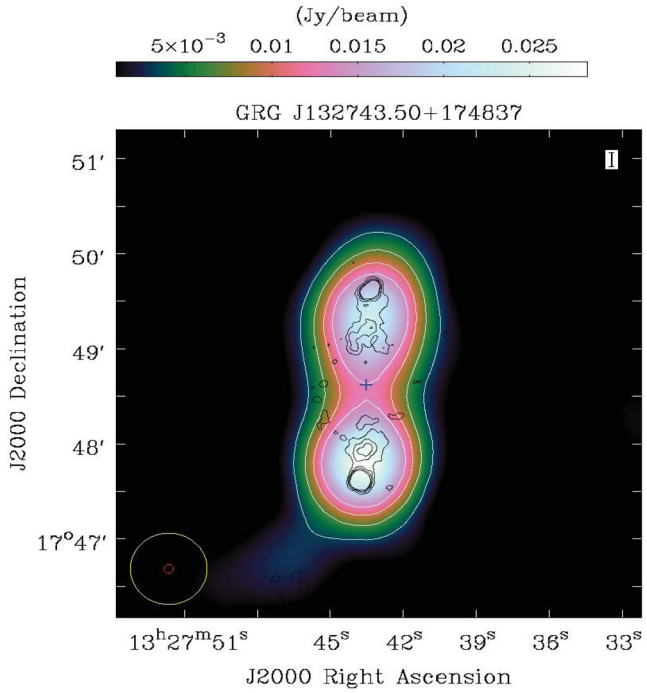

(k) **GRG11 (Linear size = 1.33 Mpc)**

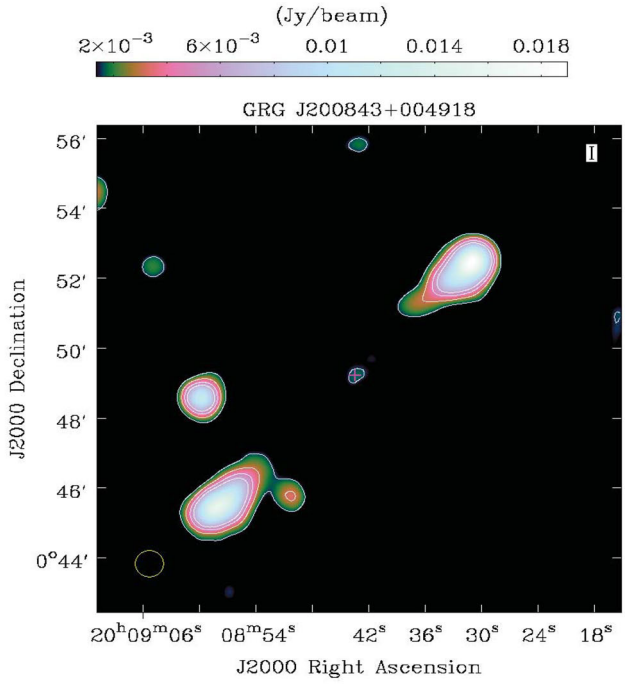

(l) **GRG12 (Linear size = 3.71 Mpc)**

Figure 1 – *Continued*

spectroscopic information from SDSS also have velocity dispersion information, which is described in detail in Bolton et al. (2012).

For GRG1, GRG2, GRG5, GRG7, GRG10 and GRG21, we adopted the classification criteria of Best & Heckman (2012) to classify the hosts into high-excitation radio galaxies (HERGs) and low-excitation radio galaxies (LERGs). If the host galaxy has [O III] (5507 Å) line equivalent width >5 Å, it is classified as a HERG else it is classified as a LERG. This is the first time that such a study of the hosts of GRGs has been attempted.

For some of the optical hosts (GRG5, GRG9, GRG13, GRG17 and GRG18), the red shifts were obtained from the 6dF galaxy survey (Jones et al. 2009). 6dF refers to the Six Degree Field instrument

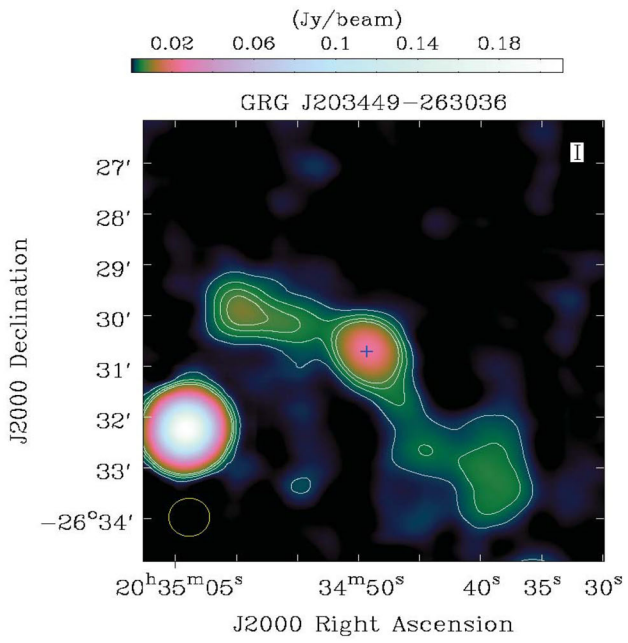

(m) **GRG13 (Linear size = 0.78 Mpc)**

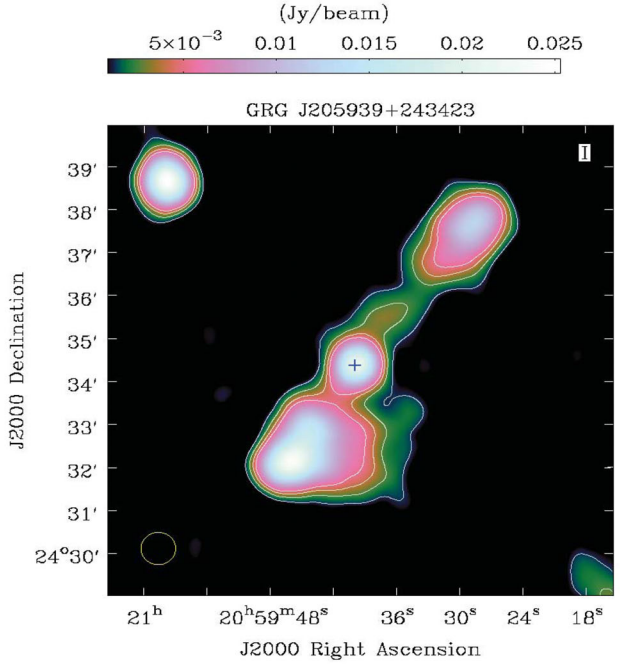

(n) **GRG14 (Linear size = 1.06 Mpc)**

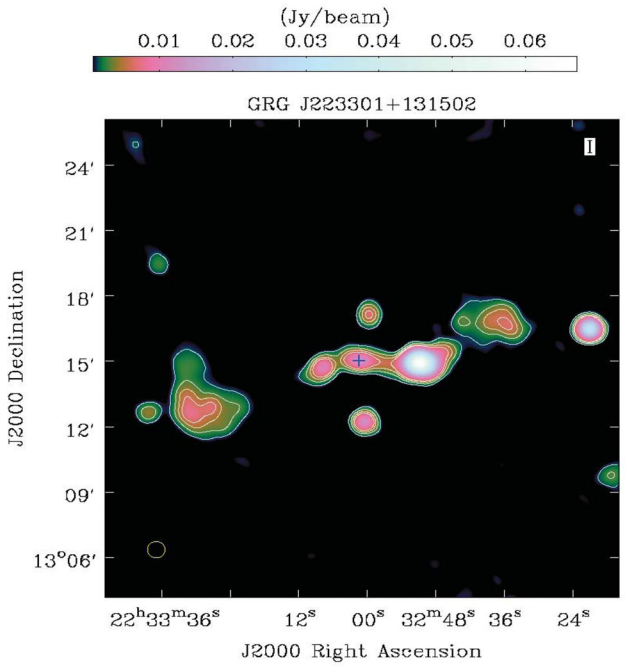

(o) **GRG15 (Linear size = 1.71 Mpc)**

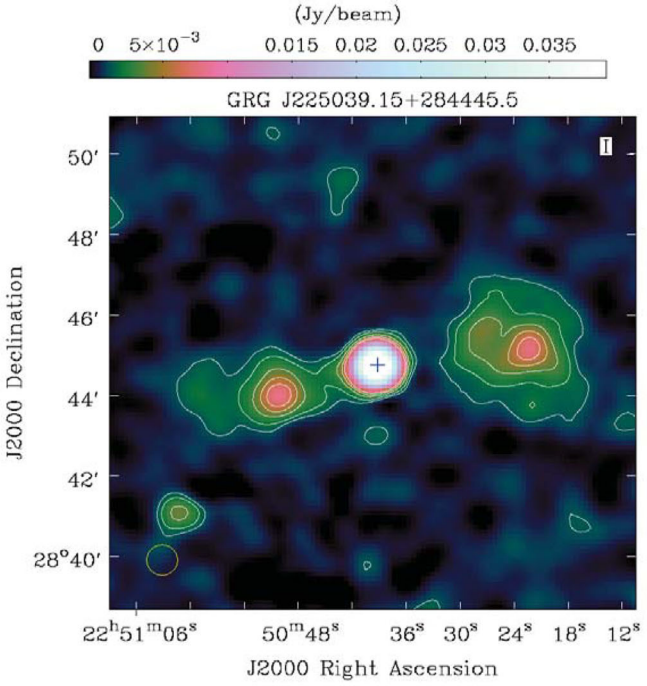

(p) **GRG16 (Linear size = 0.93 Mpc)**

Figure 1 – *Continued*

survey, which uses optical fibres and robotic positioning technology on the Anglo-Australian 3.9m telescope. The host spectrum of GRG23 was obtained from the 2MASS (Two Micron All-Sky Survey) red-shift survey (Huchra et al. 2012). For GRGs with spectroscopic host information not available in SDSS, computation of the excitation index (EI) and corresponding classification was not attempted due to either incomplete information or lower signal-to-noise ratio (SNR).

2.3 Infrared analysis

To study and classify the AGN types for the GRGs, we used the mid-IR magnitudes and colours from the *Wide-field Infrared Survey Explorer* (*WISE*) (Wright et al. 2010) for the AGN hosts of the GRGs. Colour–colour plots were used to complete this study and classification. The *WISE* survey is an all-sky survey in four mid-IR bands [W1 (3.4 μm), W2 (4.6 μm), W3 (12 μm) and W4 (22 μm)]

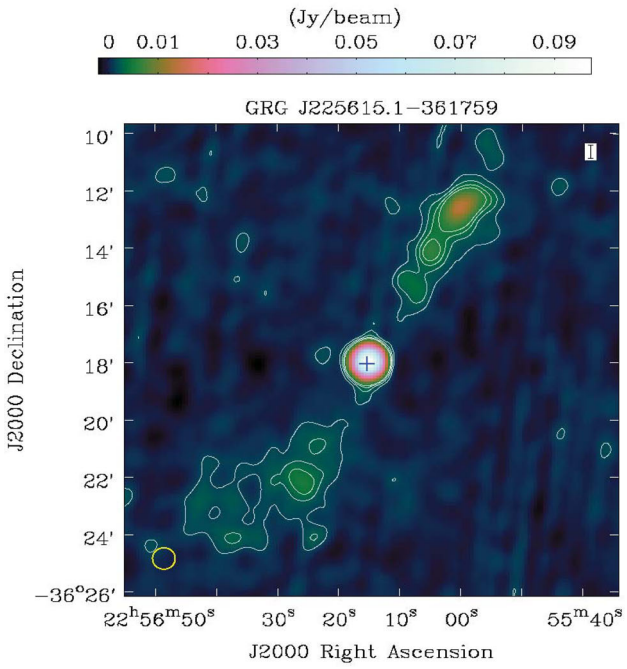

(q) **GRG17 (Linear size = 1.51 Mpc)**

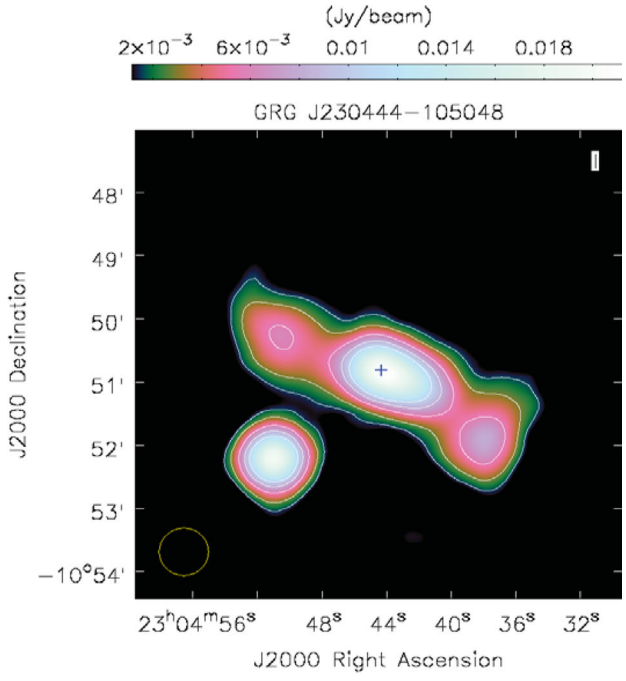

(r) **GRG18 (Linear size = 0.91 Mpc)**

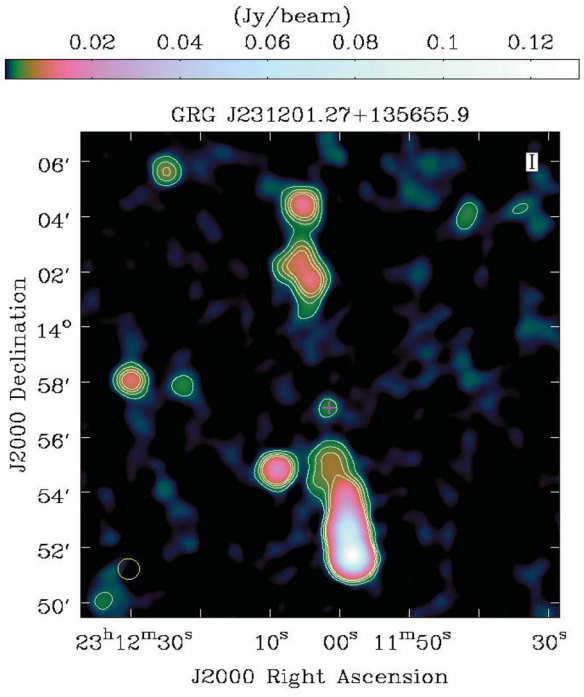

(s) **GRG19 (Linear size = 1.74 Mpc)**

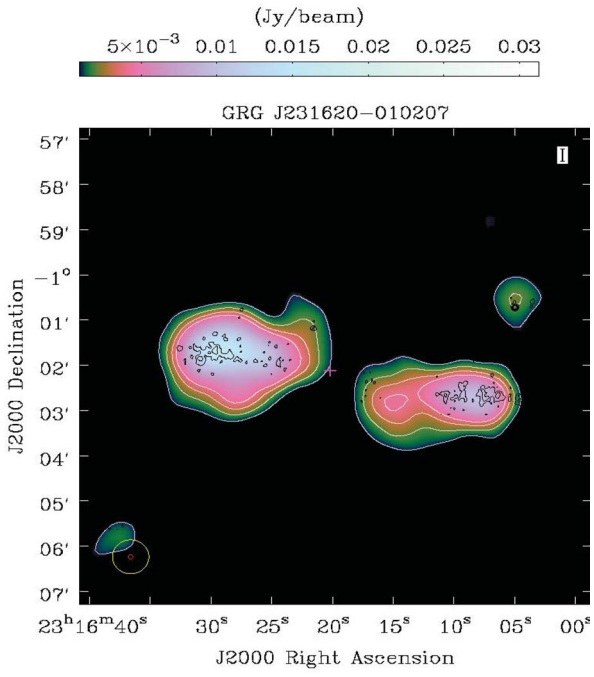

(t) **GRG20 (Linear size = 1.50 Mpc)**

Figure 1 – *Continued*

with an angular resolution of 6.1, 6.4, 6.5 and 12 arcsec, respectively. The *WISE* all-sky catalogue was searched for all the host galaxies of the GRGs in our sample within a search radius of 5 arcsec to obtain their magnitudes in the four mid-IR bands. The mid-IR magnitudes allowed us to compute the luminosities in the four respective bands (Table 4).

2.3.1 *Mid-infrared:* WISE *colour–colour plot*

We used the mid-IR colours to obtain the properties of a possibly dust obscured galactic nucleus and determine the radiative efficiency of the AGN. Mid-IR data is highly suitable for this because the optical–UV radiation from the AGN accretion disc is absorbed by the putative dusty torus and re-radiated in mid-IR bands. It has

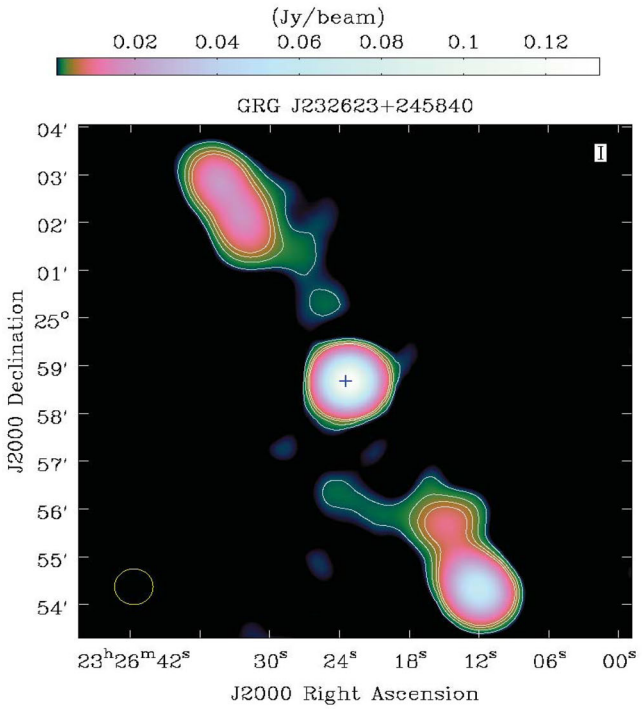

(u) **GRG21 (Linear size = 2.88 Mpc)**

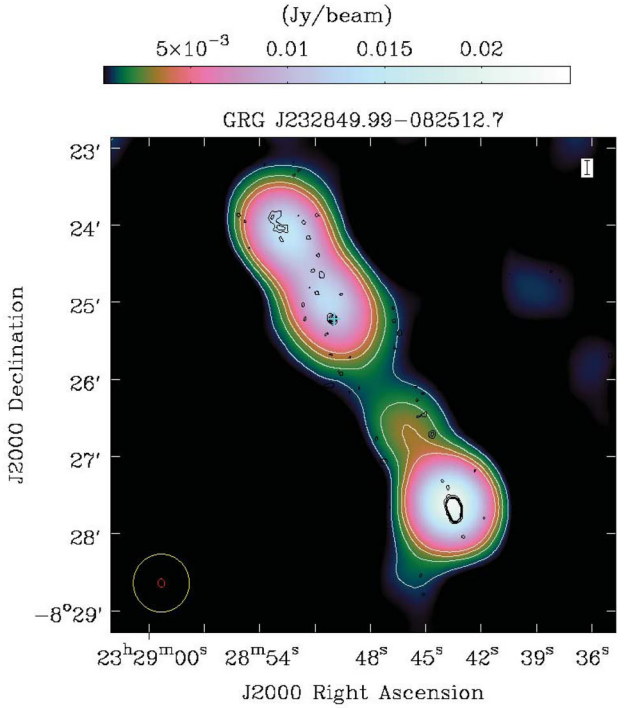

(v) **GRG22 (Linear size = 1.87 Mpc)**

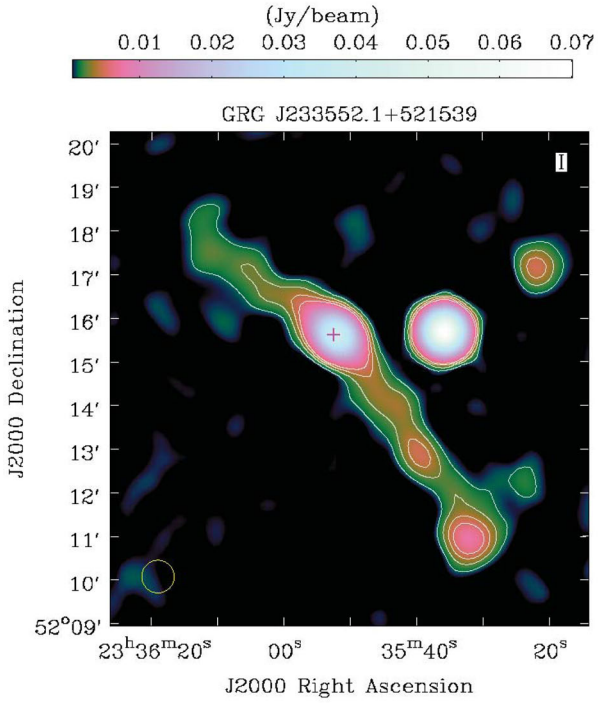

(w) **GRG23 (Linear size = 0.85 Mpc)**

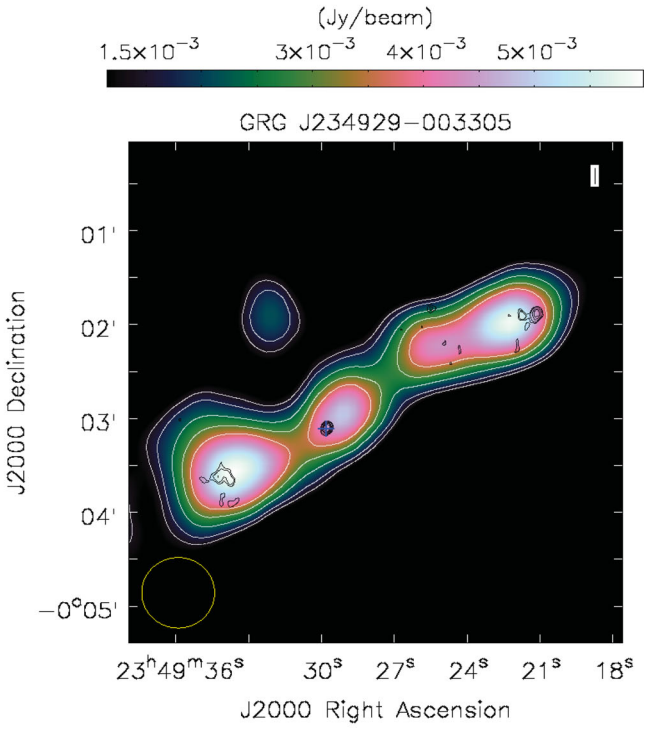

(x) **GRG24 (Linear size = 0.84 Mpc)**

Figure 1 – *Continued*

been shown that *WISE* colours can effectively distinguish AGNs from star-forming and passive galaxies. Moreover, within the AGN subset itself, HERGs and LERGs stand out clearly on the mid-IR colour–colour and mid-IR–radio plots (Lacy et al. 2004; Stern et al. 2005; Assef et al. 2010; Yang, Chen & Huang 2015). For the first time, in this paper we classify the GRGs into HERGs, LERGs, broad-line radio galaxies (BLRGs) and quasar (QSO) categories using mid-IR colours. Gürkan, Hardcastle & Jarvis (2014) showed that W1 − W2 versus W2 − W4 plots display a better separation between LERGs and narrow-line radio galaxies (NLRGs) than a W1 − W2 versus W2 − W3 plot. This in turn implies that the IR emission from the dusty torus around an AGN is possibly stronger

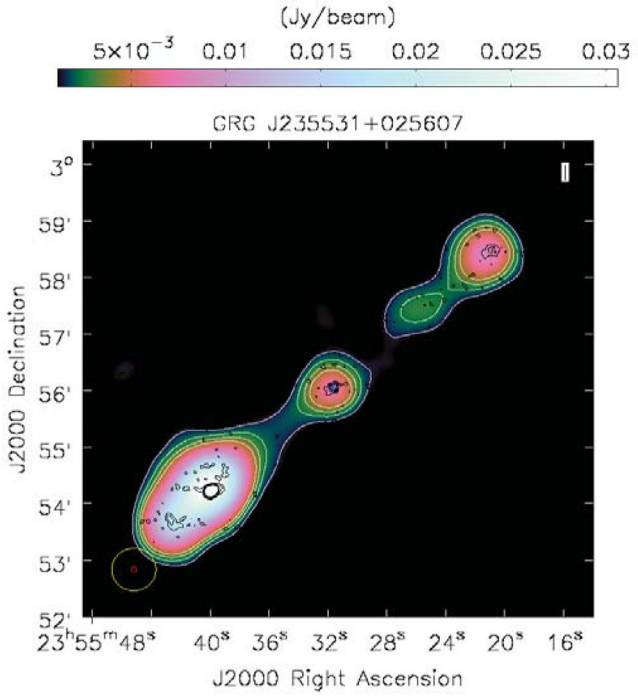

(y) **GRG25 (Linear size = 3.48 Mpc)**

Figure 1 – *Continued.*

in the W4 (22 μm) band. We produced *WISE* mid-IR colour–colour plots (like Gürkan et al. 2014) of the radio-loud AGNs associated with all our newly discovered GRGs.

2.3.2 *Near-infrared: 2MASS*

The near-IR magnitudes of the J (1.25 μm), H (1.65 μm) and K (2.17 μm) bands (Table 2) of all hosts of GRGs were obtained from the 2MASS catalogue (Skrutskie et al. 2006). The K band luminosities of the hosts of the GRGs were calculated using the K band magnitudes and red shifts. However, no data were available from 2MASS for GRG2, GRG6, GRG11, GR12, GRG15, GRG19, GRG20, GRG21, GRG22 or GRG25.

2.4 Black hole mass estimation

The central black hole mass of the host of the GRGs was computed using two methods.

2.4.1 $M_{BH} - L_{K,\,bulge}$ *relation*

The central black hole masses of the GRGs as listed in Table 2 were computed using the K band magnitude of the (bulge dominated) elliptical host galaxy ($L_{K,\,bulge}$) and using the $M_{BH} - L_{K,\,bulge}$ correlation (Marconi & Hunt 2003; Graham 2007). The absolute K band magnitude for the Sun of $M_{K,\odot} = 3.28$ was used to compute the K band bulge luminosity:

$$\log(M_{bh}/M_\odot) = 0.95(\pm0.15)\log\frac{L_{K,sph}}{10^{10.91}L_{K,\odot}} + 8.26(\pm0.11) \quad (3)$$

where $L_{K,\,sph}/L_{K,\,\odot}$ is the K band luminosity of the spheroid component of the galaxy (i.e. the bulge or the elliptical galaxy itself) in solar units.

2.4.2 $M_{BH} - \sigma$ *relation*

Information on the central velocity dispersion for the optical hosts of GRG1, GRG2, GRG7, GRG10, GRG11, GRG19 and GRG21 is available via fibre spectroscopy in SDSS DR12 (Table 3), which further enabled us to compute the central black hole mass using the well-known $M_{BH} - \sigma$ relation (McConnell & Ma 2013):

$$\log(M_{BH}/M_\odot) = \alpha + \beta\log(\sigma/200\,\mathrm{km\,s^{-1}}) \quad (4)$$

where $\alpha = 8.32 \pm 0.05$ and $\beta = 5.64 \pm 0.32$.

3 RESULTS

In this section, we provide notes on individual GRGs and discuss their optical, mid-IR and radio properties in detail.

Table 2. The J, H and K band magnitudes along with their respective errors. M_{BH} is the mass of the black hole determined using the $M_{BH} - L_{K,\,bulge}$ correlation as given in equation (3).

GRG No.	J	J_{Error}	H	H_{Error}	K	K_{Error}	M_{BH} (10^8 M$_\odot$)	$M_{BHerror}$ (10^8 M$_\odot$)
1	17.31	0.23	16.25	0.17	15.64	0.2	13.8	2.4
3	17.12	0.22	16.52	0.25	15.39	0.21	6	1.1
4	16.62	–	16.58	–	14.79	0.13	34.6	3.8
5	16.18	0.1	15.69	0.15	14.59	0.11	17	1.7
7	17.03	0.23	16.02	0.19	15.35	0.19	6.3	1.0
8	16.46	0.11	15.8	0.13	15.18	0.13	3.8	0.5
9	14.32	0.08	13.69	0.11	13.11	0.07	5.8	0.4
10	14.45	0.06	13.9	0.07	13.33	0.06	6.6	0.3
13	14.14	0.05	13.54	0.06	13.1	0.06	5.9	0.3
14	15.34	0.07	14.6	0.08	14.24	0.09	2.8	0.2
16	14.62	0.05	14.1	0.06	13.56	0.06	3.5	0.2
17	14.19	0.05	13.48	0.06	12.98	0.05	5.0	0.2
18	15.51	0.08	14.69	0.1	13.99	0.09	12	0.9
23	14.18	0.07	13.28	0.08	12.97	0.08	3.1	0.2
24	16.95	0.14	15.89	0.15	15.3	0.17	2.9	0.4

Table 3. Central velocity dispersion for hosts of GRGs whose data were available from SDSS. The velocity dispersion values were used to compute the black hole mass of the hosts of the following GRGs using the $M_{BH} - \sigma$ relation.

ID	Velocity dispersion (km s^{-1})	M_{BH} (10^9 M$_\odot$)
GRG1	169.65 ± 35.02	0.08 ± 0.09
GRG2	250.18 ± 48.54	0.73 ± 0.80
GRG7	280.21 ± 30.28	1.39 ± 0.85
GRG10	309.58 ± 07.41	2.45 ± 0.33
GRG11	286.46 ± 70.63	1.59 ± 2.2
GRG19	247.28 ± 07.35	0.69 ± 0.11
GRG21	202.82 ± 14.13	0.22 ± 0.08

3.1 GRG1 (J001604+042024)

GRG1 (Fig. 1a) is a very low surface brightness radio source (∼50 mJy) with a projected linear size of about 2.4 Mpc. The radio maps from NVSS show two radio lobes on both sides of the faint core. The host galaxy is at a red shift of 0.433 and is one of the distant GRGs in our sample. Based on the criteria suggested by Best & Heckman (2012), as mentioned in Section 2.2 we classify the host of GRG1 as a LERG.

3.2 GRG2 (J002224.96−081845)

GRG2 (Fig. 1b) is the fourth most distant GRG in our sample with a spectroscopic red shift of 0.571. This results in an overall projected linear size of ∼2.5 Mpc. Few GRGs with an overall size greater than 2 Mpc are known and there are even fewer at higher red shifts. It is the most powerful source from our sample, as shown in Table 1. The FIRST map clearly resolves the faint radio core and the two radio lobes. GRG2 can clearly be classified as a FR-II-type RG. Based on the criteria suggested by Best & Heckman (2012), as mentioned in Section 2.2 we classify the host of GRG2 as a LERG. This GRG is also mentioned in Bankowicz, Koziel-Wierzbowska & Machalski (2015), who obtained the spectroscopic red shift of the host galaxy, which is like that of SDSS as quoted above.

3.3 GRG3 (J031536−074338)

GRG3 (Fig. 1c) is one of the smallest GRGs in our sample with an overall projected linear size of about 0.86 Mpc. The FIRST map clearly resolves the radio core and lobes thereby confirming its FR-II-type nature.

3.4 GRG4 (J042925+003304): a giant radio quasar?

We observe GRG4 (Fig. 1d) to have a very high IR luminosity as seen in Table 4. GRG4 is located at a moderately high red shift of $z \sim 0.47$ (SDSS photoZ). Fig. A2 shows the host galaxy exhibiting a prominent red colour, which could be attributed to obscuration by dust. This could be a possible reason why this galaxy has acquired such a large IR luminosity. Using the 2MASS *K* band bulge luminosity, we computed the mass of the central black hole to be massive at $\sim 3.5 \times 10^9$ M$_\odot$. Based on the high mass of the central black hole and the high luminosities in the radio and IR bands, we infer GRG4 to be a QSO; however, a high-sensitivity optical spectrum is still needed to confirm its QSO nature. Our claim is further supported by its position on the *WISE* mid-IR colour–colour plots as seen in Fig. 6. The AGN clearly lies in a region on the plot that is populated mostly by radio-loud QSOs. The host galaxy also could be an ultra-luminous IR galaxy with its far-IR luminosity above 10^{12} L$_\odot$, as seen in Table 4.

Table 4. Mid-IR band magnitudes of GRGs. SNR is the profile-fit measurement signal-to-noise ratio in that band. This value is the ratio of the flux (of the band) to the flux uncertainty in the W1 profile-fit photometry measurement. Column 10 shows the classification of the GRGs using the mid-IR *WISE* scheme, whereas column 11 shows the GRG classification based on optical line flux ratios from the SDSS spectrum. The *WISE* mid-IR luminosities (L_{W1}, L_{W2}, L_{W3} and L_{W4}) of GRGs in the W1, W2, W3 and W4 bands are expressed in L$_\odot$.

GRG No.	W1	W1snr	W2	W2snr	W3	W3snr	W4	W4snr	IR	Optical	L_{W1} (10^9)	L_{W2} (10^9)	L_{W3} (10^{10})	L_{W4} (10^{11})
1	14.9	31.6	14.7	16.2	12.3	2.6	8.5	1	LERG	LERG	3.38	3.84	3.68	1.2
2	14.9	31.9	14.8	16.5	12.4	−2	8.9	0.1	LERG	LERG	6.51	7.37	6.62	1.6
3	14.7	35.7	14.2	26.1	11.4	5.9	8.2	3.5	LERG	–	1.28	2.08	2.69	0.53
4	12.6	45.5	11.2	51.7	8.3	41.1	5.9	24	QSO	–	32.98	122.18	169.27	15.89
5	13.8	42.4	12.5	47.5	9.6	30.3	7.2	12.7	QSO	QSO	4.36	13.82	21.68	1.99
6	15.5	25.1	14.8	18.4	10.9	8.8	7.7	7.1	LERG	–	5.82	10.03	36.4	7.68
7	14.8	32.4	14.6	18.1	12.4	2.3	8.9	−0.3	LERG	LERG	1.27	1.53	1.19	0.27
8	14.4	39.2	13.7	30.4	11.6	3.3	8.1	1.3	HERG	–	0.92	1.77	1.17	0.3
9	12.2	47.2	12.1	47.6	11.3	6.6	8.7	0.5	LERG	–	1.59	1.71	0.35	0.04
10	12.5	47.9	12.4	48.7	11.2	9.1	8.5	3.7	LERG	LERG	1.62	1.86	0.56	0.07
11	15.4	29.3	15.2	12.6	12.4	1.1	9.1	0.6	LERG	–	5.65	6.66	9.08	1.87
12	16.9	9.3	16.4	3.9	12.5	−0.7	8.9	−0.6	LERG	–	0.47	0.76	2.59	0.75
13	12.3	47.8	12.3	42.1	11.5	4.7	8.5	0.5	LERG	–	1.37	1.43	0.3	0.05
14	13.6	44.1	13.4	38.6	11.5	6	8.8	0.4	LERG	–	0.57	0.67	0.41	0.05
16	12.7	44.6	12.6	43.1	11.0	8.7	8.7	2.7	LERG	–	0.84	0.97	0.41	0.03
17	12.5	46.9	12.3	48.7	10.6	12.6	8.9	0.5	LERG	–	0.93	1.04	0.55	0.03
18	13.4	38.6	13.2	29.9	11.6	1.1	7.8	1.8	LERG	–	2.58	3.16	1.31	0.45
20	14.9	31.5	13.9	25.8	11.0	7.2	8.1	1.4	QSO	–	0.69	1.74	2.52	0.36
21	14.5	35.5	13.9	30.5	11.4	7.3	8.6	3.4	HERG	HERG	1.41	2.38	2.47	0.33
22	14.4	36.9	12.9	39.7	9.6	20.6	6.7	14.2	QSO	–	10.07	37.02	81.36	11.19
23	12.1	36.8	12.0	38	11.1	7	8.5	0.4	LERG	–	0.81	0.84	0.19	0.02
24	14.7	32.6	14.2	19.6	11.3	5.2	8.0	1.5	LERG	–	0.57	0.94	1.3	0.27
25	16.1	16.7	15.9	5.9	12.2	2.9	8.7	2.6	LERG	–	2.92	3.31	11.39	2.75

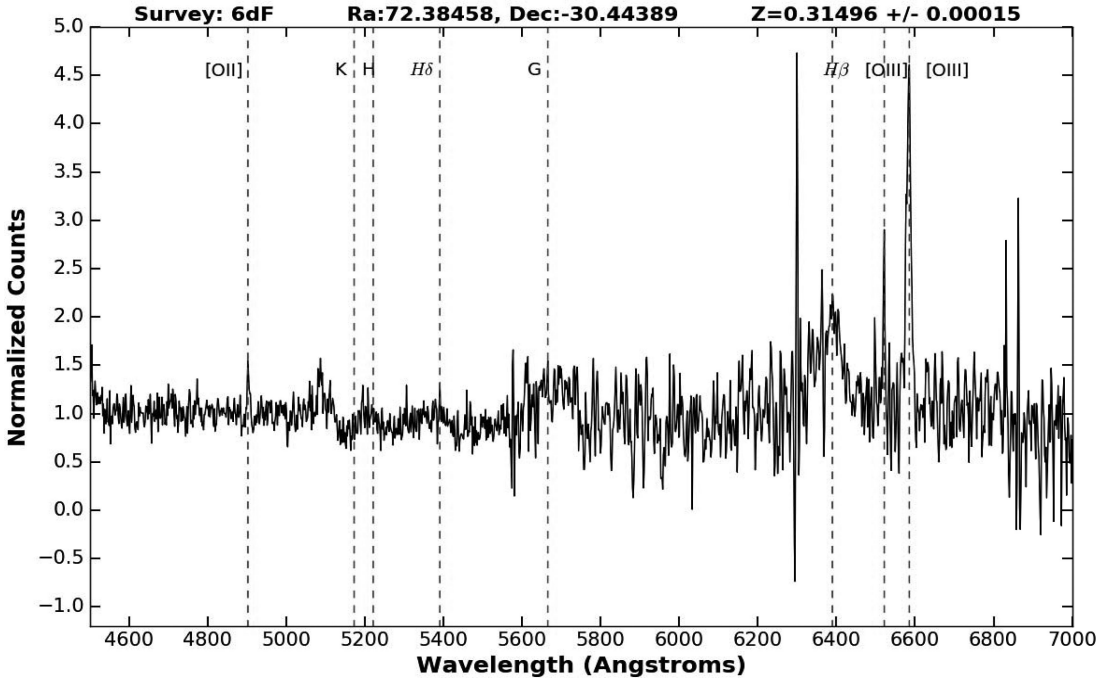

Figure 2. Replotted optical spectrum of GRG5 using 6dFGS data.

3.5 GRG5 (J044932−302638): a giant radio quasar

GRG5 has a strong core-dominated feature along with a double-lobe structure as seen in Fig. 1(e). The southern lobe is possibly contaminated by another unrelated radio source as it shows an apparent extension towards the western side. This object is also observed in the SUMSS, which is slightly poorer in resolution and sensitivity compared to NVSS. The spectroscopic red shift of ∼0.315 was obtained from Jones et al. (2009) from which the projected linear size is ∼2.1 Mpc. We infer the central black hole to be massive at 1.7×10^9 $M_\odot$ (Table 2). On the *WISE* mid-IR colour–colour plots (Fig. 6), GRG5 lies in the region of high-excitation radio-loud QSOs, which possibly makes it a giant radio QSO (GRQ). The following properties further support the hypothesis of GRG5 being a GRQ:

(i) The host galaxy of GRG5 shows excess emission in the near- and far-UV (GALEX, Bianchi & GALEX Team 1999).

(ii) It shows very high total and core (3.8×10^{24} W Hz^{-1}) radio luminosities along with high IR luminosity, which is consistent with the nature of a QSO.

(iii) The optical spectrum (Fig. 2) available in the 6dF Galaxy Survey (6dFGS, Jones et al. 2009) shows a very broad H β linewidth (∼2000 km s^{-1}), which is commonly observed in QSOs. A Gaussian fit routine with IRAF (IMAGE REDUCTION AND ANALYSIS FACILITY) and IDL (INTERACTIVE DATA LANGUAGE) on the lines of the H β and [O III] doublet of the same spectrum was used to obtain the widths, as shown in Fig. 3.

3.6 GRG6 (J080248+492723)

GRG6 (Fig. 1f) has a projected linear size of about 1.88 Mpc and its host galaxy is at a red shift of ∼0.678. This is the most distant GRG in our sample. Not many GRGs of this size are known at higher red shifts. The FIRST map clearly resolves the radio core and lobes. The black hole mass of the host is unknown due to the non-availability of the *K* band and SDSS data. The FIRST map clearly resolves this GRG, depicting its FR-II nature.

3.7 GRG7 (J085701.76+013130.9)

GRG7 (Fig. 1g) has a very low surface brightness and an overall linear size of ∼1.6 Mpc. The FIRST map clearly resolves the radio core and the two radio lobes, thus confirming its FR-II-type nature. Also, the host galaxy is located ∼3.5 arcmin away from the GMBCG J134.30444+01.56066 galaxy cluster (which is at a similar red shift as that of the GRG), as listed in the GMBCG catalogue of galaxy clusters (Hao et al. 2010).

3.8 GRG8 (J105838.66+244535)

GRG8 (Fig. 1h) shows a peculiar morphology extending over 2.1 Mpc. The southern lobe is highly diffuse with an integrated flux (S_i) of just ∼30 mJy at 1.4 GHz. In contrast to the southern lobe, the northern lobe shows a typical edge-brightened lobe with an integrated flux (S_i) of ∼120 mJy.

3.9 GRG9 (J105920−170920)

GRG9 (Fig. 1i) shows clear FR-II-type morphology extending over 1 Mpc. The overall integrated flux (S_i) of GRG9 is only about 150 mJy at 1.4 GHz and it has traces of diffuse emission.

3.10 GRG10 (J132741+574943)

The radio core of GRG10 shows an extension towards the southern lobe, which could be attributed to an unresolved radio jet. Interestingly, from Fig. 1j, we observe diffuse emission beyond the hotspot of the northern lobe. The radio core as detected in FIRST coincides with the galaxy SDSS J132741.32+574943.4, thus confirming it as a host. It is at a spectroscopic red shift of 0.1202, which makes its projected linear size 1.6 Mpc.

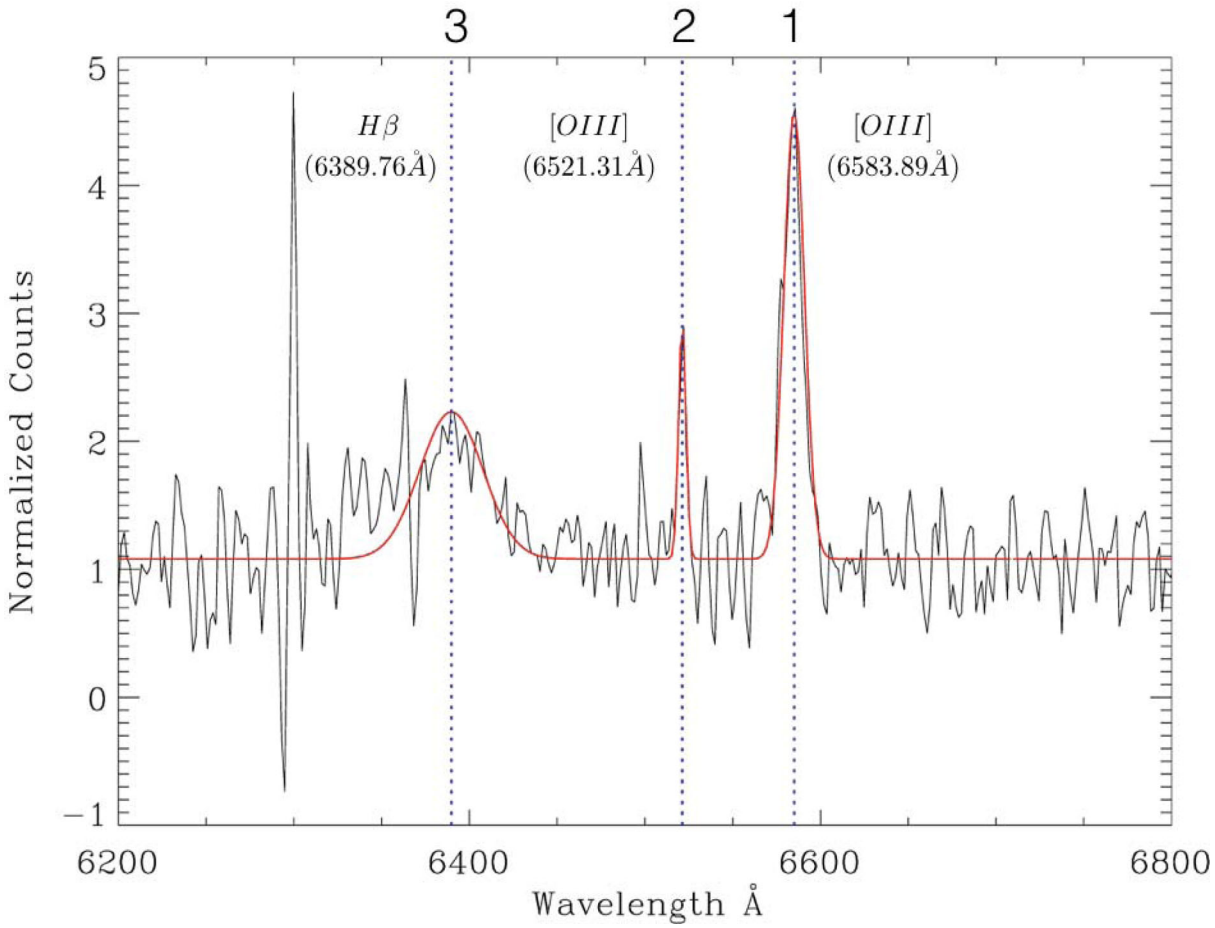

Figure 3. Zoomed-in version of the optical spectrum of the host of GRG5 (J044932−302638) obtained from 6dFGS. A Gaussian was fitted to the spectral lines of the H β and [O III] doublet to obtain the widths. The widths are as follows: (1) [O III]: $\Delta\lambda = 13.77$ Å, $\Delta v = 627.3$ km s^{-1}, (2) [O III]: $\Delta\lambda = 4.91$ Å, $\Delta v = 226.3$ km s^{-1}, (3) H β: $\Delta\lambda = 42.39$ Å, $\Delta v = 1990.2$ km s^{-1}. The broad nature of the H β line is a clear indicator of its QSO nature.

3.11 GRG11 (J132743.50+174837)

GRG11 is one of the more distant GRGs in our sample with a red shift of ∼0.657. The FIRST map (Fig. 1 k) resolves GRG11 to be of FR-II type with distinctive lobes. The host galaxy appears highly reddened (Fig. A2). We obtain a massive $\sim 10^9$ M$_\odot$ black hole mass via $M_{\rm BH} - \sigma$, but this should be treated with caution due to the high error, as seen in Table 3.

3.12 GRG12 (J200843+004918): an extremely large radio source?

GRG12 has an angular size of 11 arcmin ahd it has a strong edge-brightened FR-II structure. A faint galaxy, SDSS J200843.37+004918.8 ($m_r = 20.76$), coincides with the faint radio core as seen in Fig. 1(l), indicating it to be the host galaxy of GRG12. The host galaxy has a photometric red shift of 0.412 (SDSS photoZ), which results in a linear size of ∼3.7 Mpc. This would make GRG12 the largest GRG in the present sample as well as one of the largest radio sources known to date, after GRG J0422+1512 (∼4 Mpc) (Amirkhanyan, Afanasiev & Moiseev 2015), 3C236 (∼4.6 Mpc) (Willis et al. 1974) and GRG J1420−0545, the biggest with a projected linear size of ∼4.9 Mpc (Machalski et al. 2008). The sizes of these GRGs (GRG J0422+1512, GRG 3C236 and GRG J1420−0545) were re-computed based on the cosmology adopted in this paper. RGs of such extreme physical sizes are extremely rare. GRG12 shows a clear FR-II morphology and is quite like GRG J1420−0545. The mass of the central black hole could not be determined via the $M_{\rm BH} - L_{K,\,\rm bulge}$ correlation as the host galaxy is not detected in 2MASS. It was also not detected in the *WISE* survey in any bands, suggesting the galaxy is quite far away. We need spectroscopic red-shift data and detailed radio imaging observations to probe this suspected extremely large RG further.

3.13 GRG13 (J203449−263036)

As seen in Fig. 1(m), GRG13 does not display clear lobe hotspots. The emission around the core has a more diffuse nature. The radio core is very bright, which coincides with the host galaxy 6dF J203449−263036, and it has a spectroscopic red shift of 0.103 as obtained from Jones et al. (2009). GRG13 shows a highly bent nature in the south-western lobe compared to the north-eastern lobe. Due to the presence of another strong radio source close to the north-eastern lobe, the weak diffuse emission in this region is not very clearly seen in the NVSS map. From Fig. 6, we observe GRG13 to lie in the LERG region.

3.14 GRG14 (J205939+243423)

GRG14 shows an asymmetric morphology as evidenced in Fig. 1(n). The southern lobe ($S_i = 58$ mJy) shows a strong hotspot surrounded

by some extended diffuse emission and it is closer to the radio core than the northern lobe (S_i =23 mJy). This asymmetry could be attributed to the existence of varied IGM near the southern lobe. The host galaxy, as seen in Fig. A2, shows a slightly elongated morphology. A spectrum and spectroscopic red shifts are not available for the host (SDSS J205939.82+243423.9) of GRG14. However, SDSS photoZ is about 0.116, which results in a projected linear size of ∼1.1 Mpc. Based on Fig. 6 and the low black hole mass (Table 2), we infer GRG14 to be a LERG.

3.15 GRG15 (J223301+131502): a GRG hosted by a brightest cluster galaxy

The radio morphology of this GRG is non-linear and peculiar. In the optical band, we observe the host galaxy SDSS J223301.30+131502.5 (Fig. A2) to coincide with the radio core, whose position is marked with a + on the NVSS colour contour map (Fig. 1o). On the western side of the core, we observe a bright unresolved peak, which we conjecture to be a bright knot structure on the jet. A similar but fainter knot is also observed on the eastern jet closer to the radio core. Beyond these two close hotspot/knots on either side of the radio core are the outer lobes of GRG15, which appear quite diffuse. The distance between the outer lobes is measured to be ∼16 arcmin, while the host galaxy has a photometric red shift of 0.093, which makes the projected linear size of the source 1.71 Mpc. No FIRST data are available for this source, therefore, a higher resolution image is required to extract a clear picture of its fairly complicated morphology.

Interestingly, in the GMBCG catalogue of galaxy clusters (Hao et al. 2010), we find the host of GRG15 listed as the brightest cluster galaxy (BCG) in cluster GMBCG J338.25544+13.25070. This is a bright cD galaxy (SDSS m_r = 15.21) near the cluster centre. The host is also listed as a BCG in the maxBCG galaxy cluster catalogue (Koester et al. 2007) and the WHL galaxy cluster catalogue (Wen, Han & Liu 2012). The SDSS shows the red shift of the cluster is near to 0.102, close to the photometric red shift (0.093) of the host cD galaxy. With its peculiar radio morphology and residing in a dense cluster environment, we find GRG15 to be very unusual and thus important for understanding the evolution of GRGs in dense cluster environments. Further studies are required to understand the physical and spectral evolution of this galaxy, which has attained a projected linear size of 1.71 Mpc despite being in a dense cluster environment (Fig. 5). This GRG challenges one of the common beliefs that GRGs grow to their gigantic sizes due to their preferential location in the sparse galactic environment. This GRG also demonstrates that environment alone may not play a primary role in the growth of GRGs, as commonly believed in earlier works. Rather, a powerful AGN is at work here. While it is well known that BCGs preferentially have radio-loud AGNs (Bagchi & Kapahi 1994; Best et al. 2007), observations so far imply that a very small fraction of BCGs have large-scale radio structures. This result highlights the need for more detailed studies of the external environments for other GRGs as well as the physical conditions for the black holes powering these massive objects such as their mass, spin and mass-accretion rate. This can be achieved via future high-resolution X-ray, optical and IR spectroscopic studies of the host galaxies of these GRGs.

3.16 GRG16 (J225039.15+284445.5)

The radio core coincides with the optical host perfectly (SDSS J225039.15+284445.5), which is at a red shift of ∼0.097, thus making its projected linear size 0.9 Mpc. In Fig. 1(p), we see evidence of hotspots in the source. These are asymmetric. We also observe diffuse emission beyond the hotspots.

3.17 GRG17 (J225615.1−361759)

GRG17 has a highly diffuse nature with its southern lobe more diffuse than the northern one (Fig. 1q). The northern lobe has some hint of a hotspot while the southern one is highly diffuse and has a very low surface brightness. The red shift from Jones et al. (2009) is 0.09, which makes its projected linear size as 1.5 Mpc. Only the core is significantly observed in the SUMSS.

3.18 GRG18 (J230444−105048)

GRG18 has low surface brightness and does not show clear hotspots, as seen from Fig. 1(r). Its radio core is seen to coincide with its optical host (2MASX J23044483−1050474). The red shift, obtained from Jones et al. (2009), is about 0.21, which results in a linear projected size of ∼0.9 Mpc. With no clear lobes or hotspots observed, it is more likely to be of FR-I nature.

3.19 GRG19 (J231201.27+135655.9)

The radio core coincides with the optical host (SDSS J231201.27+135655.9) and is at a red shift of ∼0.140, which results in a projected linear size of ∼1.7 Mpc. In Fig. 1(s), we observe the southern lobe to be brighter than the northern lobe. The northern lobe shows a hotspot towards the far end. Based on the criteria mentioned in Section 2.2, we classify the host of GRG19 as a LERG.

3.20 GRG20 (J231620−010207)

In Fig. 1(t), we see the distinct lobes of GRG20 with the radio core off-centre towards the eastern lobe. The radio core, as seen in FIRST, coincides with the optical host (SDSS J231620.15−010207.3). The red shift of 0.221 (SDSS photoZ) gives a projected linear size of 1.5 Mpc. In the *WISE* colour–colour diagram, we observe it to lie in the QSO region. Further optical studies are required to confirm the true nature of the host galaxy.

3.21 GRG21 (J232623+245840)

Having an extremely large size of 2.9 Mpc, GRG21 is the third largest in our sample. We obtained the spectroscopic red shift (0.2549) and velocity dispersion (σ = 202.82 ± 14.14 km s^{-1}) from its SDSS DR12 spectrum. Using the $M_{\rm BH} - \sigma$ relation, we computed the mass (Table 3) of the central black hole to be 0.22 ± 0.08 × 10^9 $M_\odot$. It has a high core radio luminosity, $L_c = 2 \times 10^{25}$ W Hz^{-1}, as computed from the NVSS maps. Based on the criteria mentioned in Section 2.2 and the mid-IR colour–colour plot (Fig. 6), we classify it as a HERG. GRG21 is a highly core-dominated RG having a bright double structure with the southern lobe (having a hotspot) being brighter (S_i = 89 mJy) than the northern lobe (S_i = 44 mJy), as seen in Fig. 1(u).

3.22 GRG22 (J232849.99−082512.7)

At a red shift of ∼0.555, its measured projected linear size is 1.9 Mpc, and the host galaxy (SDSS J232849.99−082512.7) coincides with the radio core perfectly. From Fig. 1(v), we observe that GRG22 is highly asymmetric and the radio core lies towards

the northern lobe. The core is clearly resolved in FIRST and can be seen from the black contours plotted in Fig. 1(v). This GRG is also mentioned in Bankowicz et al. (2015), who obtained the spectroscopic red shift of the host galaxy. Their value is less than that from SDSS quoted above. Taking from Bankowicz et al. (2015) the red shift for the host J232849.99−082512.7 as 0.3839 ± 0.0073, we obtain a slightly smaller projected linear size of ∼1.5 Mpc and $P_{1.4\,\mathrm{GHz}} \sim 1.8 \times 10^{25}\,\mathrm{W\,Hz^{-1}}$.

3.23 GRG23 (J233552.1+521539)

The host 2MASX J233552.14+521538.7 coincides with the radio core and is observed to be towards the north-eastern lobe. With a red shift of ∼0.07 (Huchra et al. 2012), its projected linear size measures 0.85 Mpc. From Fig. 1(w), we observe GRG23 to be an asymmetric GRG with the south-western lobe being very elongated and showing a hotspot. However, there is no indication of a hotspot in the north-eastern lobe and the jets terminate abruptly without a lobe or hotspot.

3.24 GRG24 (J234929−000305)

The host galaxy (SDSS J234929.77−000305.8) for GRG24 coincides with the radio core, which is prominently seen in FIRST. With a red shift of ∼0.187, its projected linear size measures 0.84 Mpc. From Fig. 1(x), we observe that the eastern lobe has further diffuse emission while the western lobe is elongated. The black contours seen in Fig. 1(x) are from FIRST, where the core is clearly resolved.

3.25 GRG25 (J235531+025607)

GRG25 is the second largest GRG and one of the more distant in our sample. The SDSS photoZ has red shift ∼0.657, thus giving the projected linear size as ∼3.5 Mpc. There are scarcely any GRGs known at this red shift with sizes greater than ∼2 Mpc. We observe that the host galaxy (SDSS J235531.63+025607.1) coincides with the radio core. This GRG shows a double-lobed morphology, as evidenced from Fig. 1(y). The black contours in Fig. 1(y) are from FIRST, where the core is clearly resolved.

4 DISCUSSION

4.1 Black hole mass of a GRG

It is commonly observed that megaparsec-scale RGs are hosted by bright elliptical galaxies, with a few rare exceptions recently discovered where the host galaxies are clearly spirals (Hota et al. 2011; Bagchi et al. 2014). It is conjectured that a GRG host contains a SMBH of mass 10^8–$10^9\,\mathrm{M_\odot}$ in their galactic centre, which is responsible for powering the large-scale jets and terminal lobes (Begelman et al. 1984). It still remains a mystery as to how this system of jets and lobes can grow to their current gigantic sizes. Our knowledge about the physics of black hole growth in AGNs, and the impact of the energetic relativistic jets on the surrounding medium, is very limited and not yet fully understood. Several papers have pointed out (e.g. Laor 2000; McLure et al. 2004; Sikora, Stawarz & Lasota 2007) that AGNs harbouring black holes of masses above a few $\times\ 10^8\ \mathrm{M_\odot}$ in elliptical galaxies only are capable of launching large-scale (>100 kpc) radio jets.

In our present sample, almost all the GRGs are hosted by elliptical galaxies and we show that almost all of them host SMBHs of mass range 10^8–$10^9\ \mathrm{M_\odot}$, as shown in Tables 2 and 3. The mass of the SMBH of all the GRGs, except GRG2, GRG10, GRG11, GRG12, GRG15, GRG19 to GRG22 and GRG25, was computed using the $M_{\mathrm{BH}} - L_{K,\,\mathrm{bulge}}$ correlation (Graham 2007). Interestingly, none of the black hole masses estimated by us fall below $10^8\ \mathrm{M_\odot}$, thus supporting the earlier results suggesting that there is possibly a minimum black hole mass that separates radio-loud galaxies from radio-quiet ones. Amongst our sample of 25, the mass of the central black hole of GRG1, GRG4, GRG5 and GRG18 (Table 2) is exceptionally high, all above $10^9\ \mathrm{M_\odot}$.

4.2 Demographics of GRGs

From the literature, very few GRGs are known to date (∼300) relative to normal RGs and a small subset of GRGs are known to be at high red shifts ($z > 0.8$). The effect of inverse Compton losses on the ageing of the particles in radio lobes rapidly increases with red shift, since the energy density of the cosmic microwave background increases as $(1 + z)^4$ (Peebles 1994), which when combined with adiabatic expansion and synchrotron losses, diminishes the luminosity of an object rapidly, thus making it difficult to be detected in flux-limited surveys. Therefore, this indicates that the detected high-red-shift GRGs are intrinsically very powerful. This is reflected in our sample of 25, as we have seven GRGs with red shift ≥0.3.

In Fig. 4, we compare the red-shift distributions of our GRGs (25) with other samples of known GRGs. These samples of known GRGs (Leahy, Bridle & Strom 1996; Subrahmanyan et al. 1996; Ishwara-Chandra & Saikia 1999; Schoenmakers et al. 2001) were chosen for uniformity. Their characteristics, like linear sizes and red shift, were recomputed and reconfirmed according to the cosmology adopted in this paper. Our sample of 25 GRGs clearly show a wide range of red shifts from 0.07 to ∼0.68. Due to the faint nature of GRGs, it is

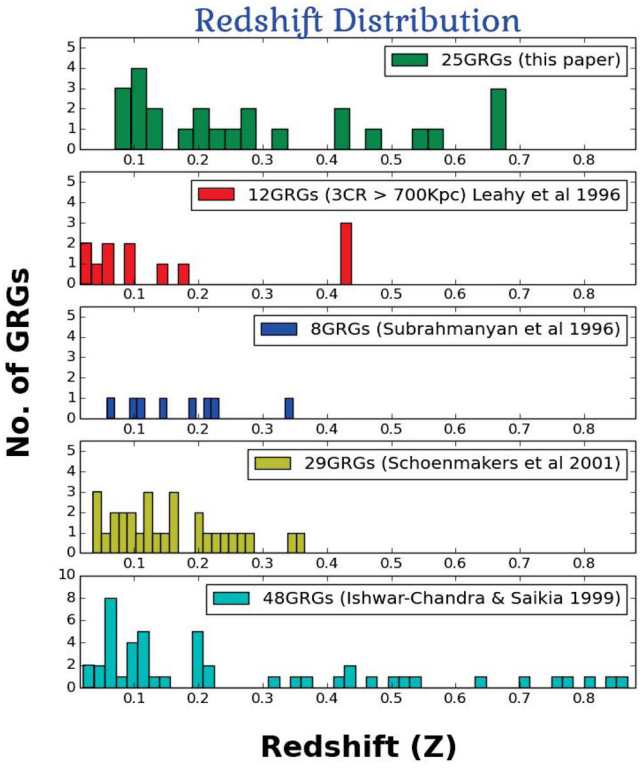

Figure 4. Comparison of the red shift distribution of GRGs of linear sizes ≥700 kpc, both from our present sample as well as from other samples of GRGs in the literature.

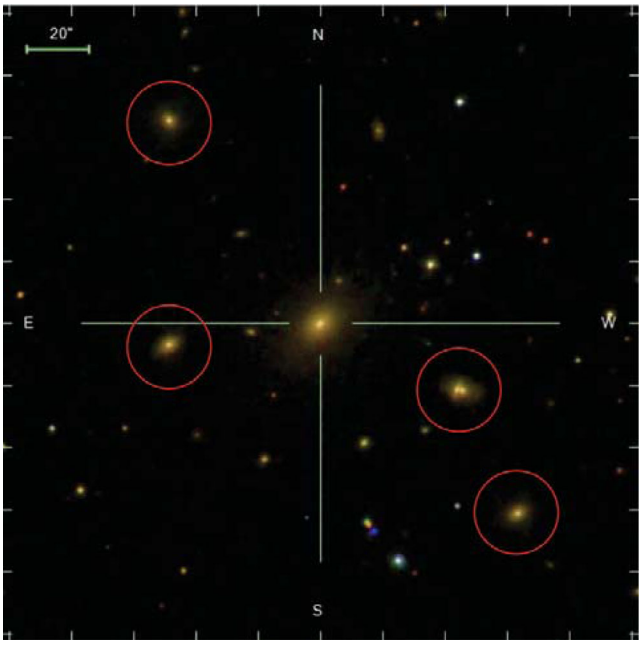

Figure 5. 3.3 × 3.3 arcmin optical SDSS image of the environment of GRG15. Red circles are other galaxies in the same cluster and at the centre is the host galaxy of GRG15.

extremely difficult to detect such large distant sources at much higher red shifts ($z > 0.5$), and this needs high-sensitivity deep images at fairly low radio frequencies ($\nu < 100$ MHz) with sufficiently high resolution where these extended lobe structures shine more prominently. Upcoming low-frequency surveys from uGMRT,[2] LOFAR (van Haarlem et al. 2013), MWA (Tingay et al. 2013) and future surveys like SKA-LOW may discover many GRGs at very high red shifts. Increasing the number of such rare distant GRGs will help us to constrain the evolutionary models in cosmic time.

Based on the intensity ratios of the optical emission lines, radio-loud AGNs can be classified into two distinct populations, namely the LERGs and HERGs. Best & Heckman (2012) differentiated between the LERGs and the HERGs by the efficiency of matter being accreted on to the central black hole. It is observed that LERGs are radiatively inefficient accretors with most of the energy from the accretion being channelled into the radio jet. On the other hand, HERGs are radiatively efficient and show strong evidence of nuclear activity in the optical band. LERGs show a high black hole mass along with a low accretion rate, which is exactly the opposite for HERGs. It is clear that jets can be generated both with and without a radiatively efficient disc. As seen from Table 4 (11th column, optical), we classified six GRGs using SDSS line flux ratios and equivalent widths into HERGs and LERGs. We do not observe any trend for the hosts of the GRGs being preferentially high excitation or low excitation. Such a classification of a large sample of GRGs will, perhaps, reveal the underlying dichotomy or any other trends for GRGs.

4.3 *WISE* mid-IR studies of GRGs

Gürkan et al. (2014) differentiated between LERGs, HERGs, NLRGs, BLRGs and radio-loud QSOs with the help of *WISE* (mid-IR) colour–colour plots using the Cambridge radio surveys (3C, 4C etc.). We place our GRGs on the *WISE* mid-IR colour–colour plots (Fig. 6) to classify their AGNs using the four mid-IR bands. To our knowledge, this is the first time this kind of classification has been done for GRGs. Gürkan et al. (2014) showed that LERGs have redder colours and lie at the bottom left region of the *WISE* colour–colour plots. From Fig. 6, we observe that the majority of the GRGs in our sample lie in the LERG region ([W1] − [W2] < 0.8). In Fig. 6, we also plot the excitation type of nearly 100 AGNs of GRGs and it is evident from this plot that GRGs do not show a preference towards high-excitation or low-excitation types. However, the GRQs are all of high-excitation type (see discussion below).

4.3.1 An efficient method for QSO identification

From standard AGN models, we know that optical or UV emission obscured by dusty structures around the accretion disc is re-radiated in the mid-IR. Thus, hidden QSOs can be found by mid-IR observations, such as *WISE*. Gürkan et al. (2014) showed that QSOs have higher mid-IR luminosities compared to other AGN types, which holds for a vast range of red shifts. The re-radiated optical or UV emission from the AGN dominates in the 22 μm flux (W4). Wu et al. (2012) also showed using SDSS QSOs that *WISE* bands are efficient for finding QSOs. From the colour–colour plots in Gürkan et al. (2014), we observed that radio-loud QSOs cluster in one particular region, defined by [W1] − [W2] > 0.85 and [W2] − [W3] > 2. We further validated this since 44 known GRQs from Kuźmicz & Jamrozy (2012) lie in the QSO region of the colour–colour plot as mentioned above. Further, we observe that GRG4, GRG5, GRG20 and GRG22 from our new sample lie in the QSO region of the plots (Fig. 6), which indicates that they are possibly radio-loud QSOs.

Such QSOs are known to have a very high core radio luminosity as well as high IR luminosity, which is indeed very well exhibited by GRG4 and GRG5 of our sample. They also show a high black hole mass ($>10^9$ $M_\odot$), which is another indicator of their QSO nature. This claim is further validated by the optical spectrum of GRG5 (Figs 2 and 3). GRQs B0750+434 (size ∼2.45 Mpc, Schoenmakers et al. 2001) and HE1127-1304 (size ∼2.1 Mpc, Bhatnagar, Gopal-Krishna & Wisotzki 1998) are two of the largest GRQs known to date. This places GRG4 and GRG5 (of size 2.4 Mpc and 2.1 Mpc, respectively) from our sample amongst the largest known GRQs. These giant radio QSOs are very important for the ongoing studies of AGN unification schemes. Therefore, we show that in the absence of an optical spectrum, the *WISE* mid-IR colour–colour plots along with the radio and IR luminosities provide a good alternative method for identifying GRQs and classifying GRGs into different AGN types.

4.4 P-D diagram

Traditionally, a P-D diagram (Baldwin 1982) is a plot between radio power (P) at some fixed frequency and the linear size (D) of RGs. Using tools such as the P-D diagram, we can study the evolution of radio sources (Kaiser, Dennett-Thorpe & Alexander 1997; Ishwara-Chandra & Saikia 1999; Manolakou & Kirk 2002; Machalski, Chyzy & Jamrozy 2004).

In Fig. 7, we plot the P-D diagram for our new sample of GRGs (25) along with a sample of known GRGs from the literature (Laing, Riley & Longair 1983; Lara et al. 2001). This is one of the biggest (82) samples (new and previously known) of GRGs ever to be

[2] http://www.gmrt.ncra.tifr.res.in/gmrt_hpage/Upgrade/index.html

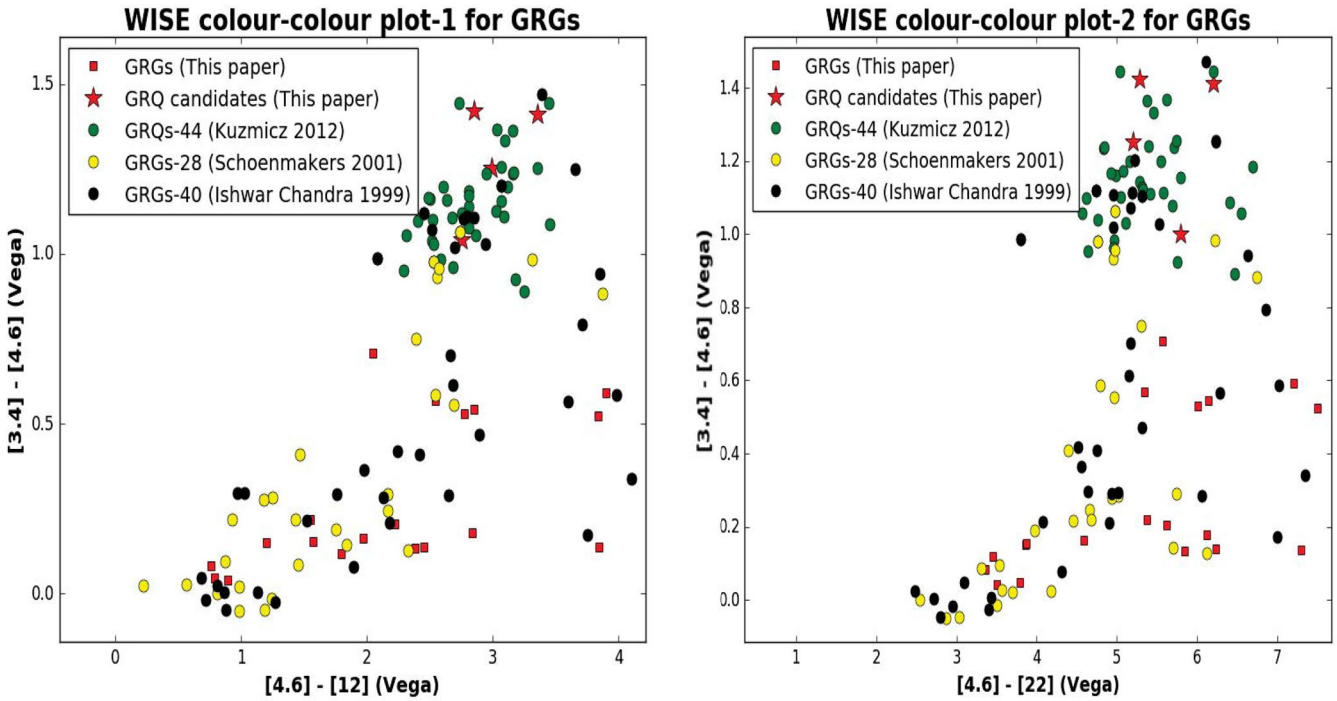

Figure 6. Our GRGs lie on the mid-IR colour–colour plots made using *WISE* mid-IR magnitudes W1, W2, W3 and W4 (3.4, 4.6, 12 and 22 μm Vega magnitudes). Left: The region of star-forming galaxies is [W2] − [W3] > 2 (Wright et al. 2010) and LERGs are concentrated mostly in the region [W1] − [W2] <0.8 and [W2] − [W3] <2.5. Right: The *x*-axis here is [W2] − [W4]. Gürkan et al. (2014) showed that in both plots, QSOs and BLRGs have similar colours.

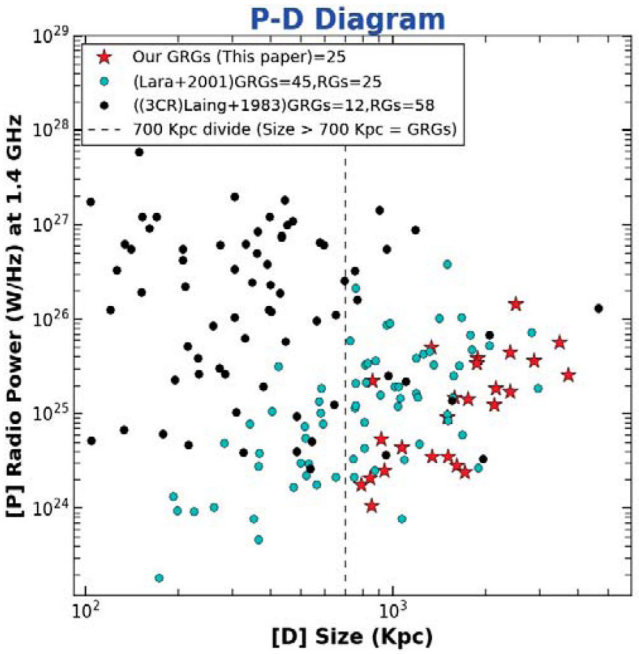

Figure 7. The 25 newly discovered GRGs plotted on a P-D diagram along with other known RGs and GRGs from different papers. Sizes and powers of known RGs and GRGs were recomputed for uniformity.

compared in a P-D diagram. For sources from 3CR,[3], the flux at 1.4 GHz was obtained using the given spectral index. This enabled us to compute the radio power at 1.4 GHz using equation (2). The 3CR sample has a total of 85 sources (DRAGNs: double radio sources associated with a galactic nucleus) of which only 70 were above 100 kpc in total size. Only these 70 sources were plotted on the P-D diagram. Based on our definition of GRGs ($D \geq 700$ kpc), only 12 sources are giants from the 3CR sample of 70 RGs. The second sample chosen for the comparison study in this plot is from Lara et al. (2001), with 70 sources (45 GRGs and 25 RGs). The sample in Lara et al. (2001) is also constructed from NVSS (like our sample) and it provided us with the 1.4-GHz flux in mJy and the total source size in arcminutes. The linear sizes and radio power were recomputed for all the objects (on the plot) using the updated cosmological parameters (as stated in Section 1) so as to maintain uniformity and avoid biases in comparison.

It is very evident from the P-D diagram that large radio sources tend to be less radio luminous at a frequency of 1.4 GHz. This, perhaps, indicates that as these RGs grow in size (megaparsec scales), they become less luminous. The diminishing luminosity is possibly due to adiabatic expansion and radiative energy losses. In some cases, it might also be because the radio-loud phase is turned off. Based on the evolutionary models by Blundell & Rawlings (1999), after an initial rapid increment, the luminosity of the radio lobes decreases rapidly as the source grows. The sources evolve towards lower power and larger size as they age. This is suggested by the absence of radio sources in the upper right corner of the P-D diagram (large sizes and high powers). Assuming that the sample used is a reasonable representation of the population, we support our claim through the results of the Mann–Whitney *U* test (Mann & Whitney 1947), which is a non-parametric test for the equality of sample medians. A galaxy size of 700 kpc is used to segregate the sample into two. Those smaller than 700 kpc are referred to as RGs while the others are GRGs. We test the null hypothesis of the median power of RGs and GRGs being equal against the alternative hypothesis of radio power of GRGs being lower than that of RGs.

[3] http://www.jb.man.ac.uk/atlas/

With the test statistic $W = 2779$ and $p = 0.0277$, we have sufficient evidence to reject the null hypothesis.

Interestingly, no sources are seen in the extreme lower right corner of the P-D diagram either, i.e. with a very large size and very low power. The surveys that have discovered most of the known GRGs so far are unable to detect these extreme GRGs due to their sensitivity limitation. The models predict that these yet unobserved sources are possibly the final stage of evolution of a RG before it fades away. Therefore, future low-frequency radio surveys (Kapinska et al. 2015) (below 100 MHz) with LOFAR, SKA-LOW etc. will be able to uncover the hitherto undetected population of giant radio sources in the bottom right part of the P-D diagram. These sources will provide vital information on the evolution of RGs to such extreme limits and on the duty cycle of accreting massive black holes in host galaxies.

Such studies of GRGs are of vital importance for making progress in understanding the unusual nature of these extreme galaxies. The multifrequency observations will allow us to obtain sensitive maps of the low surface brightness diffuse emission, spectral index maps, break frequency and spectral ages of GRGs. Under project *SAGAN*, reporting and analysis of more new GRGs from our discovery sample will form part of our next paper in this series, which is under preparation currently. Some very interesting results from a multiwavelength analysis of the larger sample of GRGs will be discussed in our consecutive papers of this same series. Recent unique work carried by others, like Proctor (2016), will be quite useful for forming a bigger and complete sample of GRGs after supplementing it with existing and new optical data. We would like to highlight that all the studies carried out in the present paper were done using archival data from various surveys in the radio, optical and IR bands.

5 CONCLUSIONS AND SUMMARY

In this paper, we present the discovery of 25 new GRGs from the NVSS survey and their multiwavelength studies. This sample of GRGs is not a complete sample from the NVSS search. Making a complete sample from these searches of NVSS is in progress and will be presented in forthcoming papers. The NVSS was completed more than 15 years ago and these new discoveries signify its continued importance and confirm that it is far from becoming obsolete. The large size and relatively low surface brightness of GRGs makes it difficult to detect them via automated detection in various radio surveys. By combining NVSS images with optical data from SDSS as well as archival data from FIRST and SUMSS, we provide a complete study of the morphology of these sources. Further, using *WISE* colours, we could classify the hosts of GRGs into different accretion types (HERGs, LERGs, etc.). Using the 2MASS *K* band and SDSS spectroscopic data, we estimate the mass of the central black hole in ∼50 per cent of hosts of these GRGs. The estimated black hole masses are in the range 10^8–10^9 $M_\odot$.

A brief summary of our results is as follows:

(i) Considering that only ∼300 GRGs are known to date, our contribution of 25 new GRGs enhances the sample by ∼9 per cent. Furthermore, all the GRGs in our sample have radio power above 10^{24} W Hz^{-1} at 1.4 GHz.

(ii) Optical spectra for 13 GRGs were available from the archive. Almost all the optical spectra presented in this paper show detection of H α, H β, [O II], [O III], N II and S II, thus confirming their AGN nature. We also classified a few GRGs as HERGs or LERGs using the SDSS line flux ratios.

(iii) We proposed a new method for identifying radio-loud QSOs without an optical spectrum. This was done by estimating the mid-IR luminosity from *WISE* and the radio luminosity and using the location on the *WISE* colour–colour plots. We find that the radio-loud QSOs cluster in one particular region of the plots defined by [W1] − [W2] > 0.85 and [W2] − [W3] > 2. We find that GRG4, GRG5, GRG20 and GRG22 show very high radio core luminosities as well as high mid-IR luminosities, which are strong indications of their QSO nature. This was further confirmed with the optical spectrum of GRG5.

(iv) We show, for the first time, the classification of GRGs into QSOs, LERGs, HERGs, etc. using the *WISE* mid-IR colour–colour plots. From this classification, we notice that nearly half of the GRGs in our sample are LERGs.

(v) None of the host galaxies of GRGs in our sample fall on the star-forming region ([W2] − [W3] ≥2.5 and [W1] − [W2] ≤ 1) of the *WISE* mid-IR colour–colour plots, from which we infer that the host galaxies of GRGs are mostly passive red ellipticals without significant star-forming activity at the present moment. However, more studies with a larger sample are required to investigate this.

(vi) GRG15 clearly challenges the common belief that GRGs grow in a sparse non-cluster environment. The optical observation of the environment of this GRG host clearly shows that it is a cD-like BCG lying in a dense central region of the cluster. This shows that the environment alone does not play a major role in their exceptional large sizes.

(vii) The P-D diagram suggests that GRGs (>0.7 Mpc), in comparison to normal RGs, are less luminous and less powerful, indicating the end stage (de-energising) of the RG lifetime. Moreover, we observe a lack of extremely large and powerful sources in the top right corner of the P-D diagram.

(viii) Also, the P-D diagram suggests a cut-off in GRG radio power at ∼10^{26} W Hz^{-1} with a drastic drop-off in linear size beyond 3 Mpc. This indicates that GRGs are large low-surface-brightness sources that show a decrease in radio power with the increase in size, as expected for the luminosity evolution of active RGs (Kaiser et al. 1997; Blundell & Rawlings 1999). Furthermore, this cut-off is possibly limited by instrumental sensitivity.

(ix) The occurrence of GRGs with respect to red shift (Fig. 4) also shows a decrease, thereby indicating the limitation in the detection of distant GRGs with current surveys. It also highlights the need for high-sensitivity low-frequency radio surveys in the near future with telescopes like uGMRT, LOFAR and SKA.

ACKNOWLEDGEMENTS

We acknowledge the comments and suggestions of the anonymous referee, which helped us to improve the quality of our paper. PD, JB and MP gratefully acknowledge generous support from the Indo-French Centre for the Promotion of Advanced Research (Centre Franco-Indien pour la Promotion de la Recherche Avancée) under programme 5204-2. We thank the people who made NVSS, FIRST and SUMSS for the radio data and SDSS and 6dF for the optical data. We thank IUCAA (especially the Radio Physics Lab), Pune, for providing all the facilities for carrying out the research work. We thank the late Dr Homi Bhabha for the inspiration. We thank Mr Tejas Kale for a discussion related to statistical tests. We gratefully acknowledge the use of Edward (Ned) Wright's online Cosmology Calculator. This research made use of the NASA Extragalactic Database (NED), which is operated by the Jet Propulsion Laboratory, California Institute of Technology, under contract with the National Aeronautics and Space Administration. This

research also made use of the SIMBAD data base, operated at CDS, Strasbourg, France. This publication makes use of data products from *WISE*, which is a joint project of the University of California, Los Angeles, and the Jet Propulsion Laboratory/California Institute of Technology, funded by the National Aeronautics and Space Administration.

REFERENCES

Alam S. et al., 2015, ApJS, 219, 12
Amirkhanyan V. R., Afanasiev V. L., Moiseev A. V., 2015, Astrophys. Bull., 70, 45
Assef R. J. et al., 2010, ApJ, 713, 970
Bagchi J., Kapahi V. K., 1994, J. Astrophys. Astron., 15, 275
Bagchi J., Durret F., Neto G. B. L., Paul S., 2006, Science, 314, 791
Bagchi J. et al., 2014, ApJ, 788, 174
Baldwin J. E., 1982, in Heeschen D. S., Wade C. M., eds, Proc. IAU Symp. 97, Extragalactic Radio Sources. Kluwer, Dordrecht, p. 21
Bankowicz M., Koziel-Wierzbowska D., Machalski J., 2015, Proc. Sci., SALT Observations of the Largest Radio Galaxies. SISSA, Trieste, PoS(SSC2015)034
Bauleo P. M., Rodríguez Martino J., 2009, Nature, 458, 847
Becker R. H., White R. L., Helfand D. J., 1995, ApJ, 450, 559
Begelman M. C., Blandford R. D., Rees M. J., 1984, Rev. Modern Phys., 56, 255
Best P. N., Heckman T. M., 2012, MNRAS, 421, 1569
Best P. N., von der Linden A., Kauffmann G., Heckman T. M., Kaiser C. R., 2007, MNRAS, 379, 894
Bhatnagar S., Gopal-Krishna Wisotzki L., 1998, MNRAS, 299, L25
Bianchi L., GALEX Team, 1999, Mem. Soc. Astron. Italiana, 70, 365
Blandford R. D., Payne D. G., 1982, MNRAS, 199, 883
Blandford R. D., Znajek R. L., 1977, MNRAS, 179, 433
Blundell K. M., Rawlings S., 1999, Nature, 399, 330
Bolton A. S. et al., 2012, AJ, 144, 144
Condon J. J., Cotton W. D., Greisen E. W., Yin Q. F., Perley R. A., Taylor G. B., Broderick J. J., 1998, AJ, 115, 1693
Donoso E., Best P. N., Kauffmann G., 2009, MNRAS, 392, 617
Enßlin T. A., Gopal-Krishna 2001, in Laing R. A., Blundell K. M., eds, ASP Conf. Ser. Vol. 250, Particles and Fields in Radio Galaxies Conference. Astron. Soc. Pac., San Francisco, p. 454
Fanaroff B. L., Riley J. M., 1974, MNRAS, 167, 31P
Graham A. W., 2007, MNRAS, 379, 711
Green D. A., 2011, Bull. Astron. Soc. India, 39, 289
Gürkan G., Hardcastle M. J., Jarvis M. J., 2014, MNRAS, 438, 1149
Hao J. et al., 2010, ApJS, 191, 254
Hardcastle M. J., Cheung C. C., Feain I. J., Stawarz Ł., 2009, MNRAS, 393, 1041
Hillas A. M., 1984, ARA&A, 22, 425
Hooper D., 2016, J. Cosmol. Astropart. Phys., 09, 002
Hörandel J. R., 2008, in Röser S., ed., Reviews in Modern Astronomy Vol. 20. Wiley-VCH, p. 198
Hota A. et al., 2011, MNRAS, 417, L36
Huchra J. P. et al., 2012, ApJS, 199, 26
Ishwara-Chandra C. H., Saikia D. J., 1999, MNRAS, 309, 100
Jamrozy M., Konar C., Machalski J., Saikia D. J., 2008, MNRAS, 385, 1286
Jones D. H. et al., 2009, MNRAS, 399, 683
Kaiser C. R., Dennett-Thorpe J., Alexander P., 1997, MNRAS, 292, 723
Kapinska A. D., Hardcastle M., Jackson C., An T., Baan W., Jarvis M., 2015, Unravelling Lifecycles and Physics of Radio-loud AGN in the SKA Era. SISSA, Trieste, PoS(AASKA14)173
Kellermann K. I., Verschuur G. L., 1988, Galactic and Extragalactic Radio Astronomy, 2nd edn. Springer-Verlag, Berlin and New York, p. A89-40410
Koester B. P. et al., 2007, ApJ, 660, 239
Kronberg P. P., 1994, Rep. Progress Phys., 57, 325
Kronberg P. P., 2004, J. Korean Astron. Soc., 37, 343
Kronberg P. P., Dufton Q. W., Li H., Colgate S. A., 2001, ApJ, 560, 178
Kuźmicz A., Jamrozy M., 2012, MNRAS, 426, 851
Lacy M. et al., 2004, ApJS, 154, 166
Laing R. A., Riley J. M., Longair M. S., 1983, MNRAS, 204, 151
Laor A., 2000, ApJ, 543, L111
Lara L., Cotton W. D., Feretti L., Giovannini G., Marcaide J. M., Márquez I., Venturi T., 2001, A&A, 370, 409
Leahy J. P., Bridle A. H., Strom R. G., 1996, in Ekers R. D., Fanti C., Padrielli L., eds, Proc. IAU Symp. 175, Extragalactic Radio Sources. Kluwer, Dordrecht, p. 157
Lynden-Bell D., 1969, Nature, 223, 690
Machalski J., Jamrozy M., Zola S., 2001, A&A, 371, 445
Machalski J., Chyzy K. T., Jamrozy M., 2004, Acta Astron., 54, 391
Machalski J., Jamrozy M., Zola S., Koziel D., 2006, A&A, 454, 85
Machalski J., Koziel-Wierzbowska D., Jamrozy M., 2007, Acta Astron., 57, 227
Machalski J., Kozieł-Wierzbowska D., Jamrozy M., Saikia D. J., 2008, ApJ, 679, 149
Malarecki J. M., Jones D. H., Saripalli L., Staveley-Smith L., Subrahmanyan R., 2015, MNRAS, 449, 955
Mann H. B., Whitney D. R., 1947, Ann. Math. Stat., 18, 50
Manolakou K., Kirk J. G., 2002, A&A, 391, 127
Marconi A., Hunt L. K., 2003, ApJ, 589, L21
Mauch T., Murphy T., Buttery H. J., Curran J., Hunstead R. W., Piestrzynski B., Robertson J. G., Sadler E. M., 2003, MNRAS, 342, 1117
McConnell N. J., Ma C.-P., 2013, ApJ, 764, 184
McLure R. J., Willott C. J., Jarvis M. J., Rawlings S., Hill G. J., Mitchell E., Dunlop J. S., Wold M., 2004, MNRAS, 351, 347
Peebles P. J. E., 1994, Am. J. Phys., 62, 381
Planck Collaboration XIII, 2016, A&A, 594, A13
Proctor D. D., 2016, ApJS, 224, 18
Rengelink R. B., Tang Y., de Bruyn A. G., Miley G. K., Bremer M. N., Roettgering H. J. A., Bremer M. A. R., 1997, A&AS, 124
Safouris V., Subrahmanyan R., Bicknell G. V., Saripalli L., 2009, MNRAS, 393, 2
Saripalli L., Hunstead R. W., Subrahmanyan R., Boyce E., 2005, AJ, 130, 896
Schoenmakers A. P., de Bruyn A. G., Röttgering H. J. A., van der Laan H., 2001, A&A, 374, 861
Sikora M., Stawarz Ł., Lasota J.-P., 2007, ApJ, 658, 815
Skrutskie M. F. et al., 2006, AJ, 131, 1163
Stern D. et al., 2005, ApJ, 631, 163
Subrahmanyan R., Saripalli L., Hunstead R. W., 1996, MNRAS, 279, 257
Subrahmanyan R., Saripalli L., Safouris V., Hunstead R. W., 2008, ApJ, 677, 63
Tingay S. J. et al., 2013, PASA, 30, e007
van Haarlem M. P. et al., 2013, A&A, 556, A2
van Weeren R. J., Röttgering H. J. A., Brüggen M., Hoeft M., 2010, Science, 330, 347
Wen Z. L., Han J. L., Liu F. S., 2012, ApJS, 199, 34
Willis A. G., Strom R. G., Wilson A. S., 1974, Nature, 250, 625
Wright E. L., 2006, PASP, 118, 1711
Wright E. L. et al., 2010, AJ, 140, 1868
Wu X.-B., Hao G., Jia Z., Zhang Y., Peng N., 2012, AJ, 144, 49
Yang X.-h., Chen P.-S., Huang Y., 2015, MNRAS, 449, 3191
York D. G. et al., 2000, AJ, 120, 1579

APPENDIX A: SOME EXTRA MATERIAL

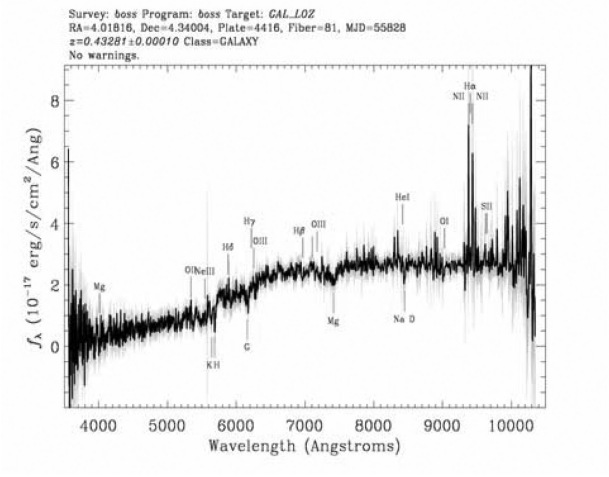

(a) **GRG1 spectrum**

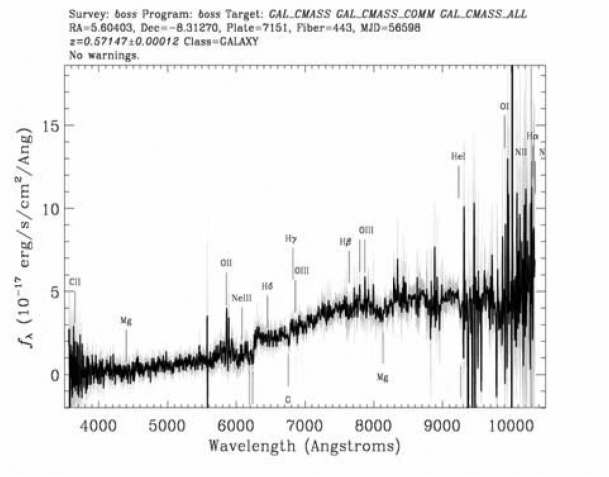

(b) **GRG2 spectrum**

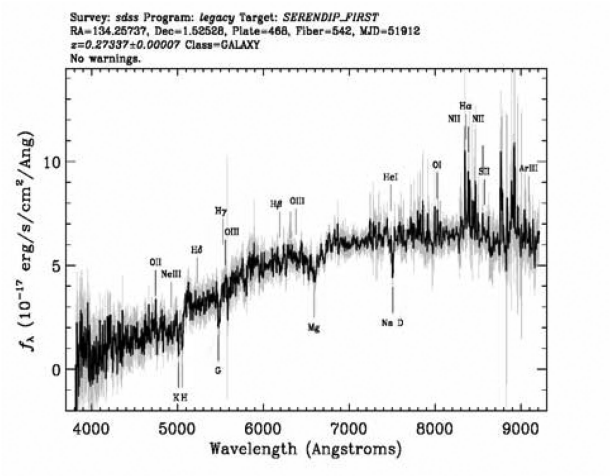

(c) **GRG7 spectrum**

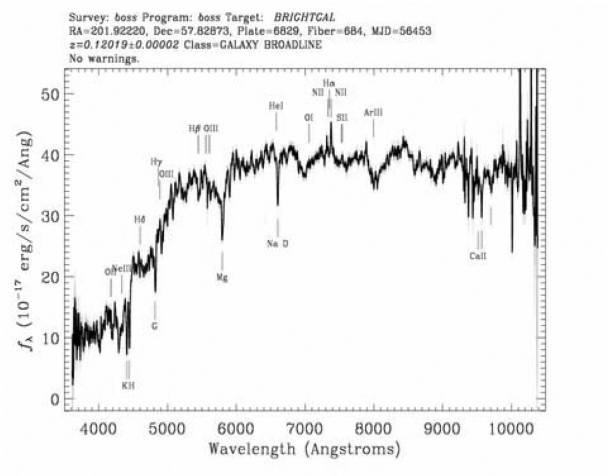

(d) **GRG10 spectrum**

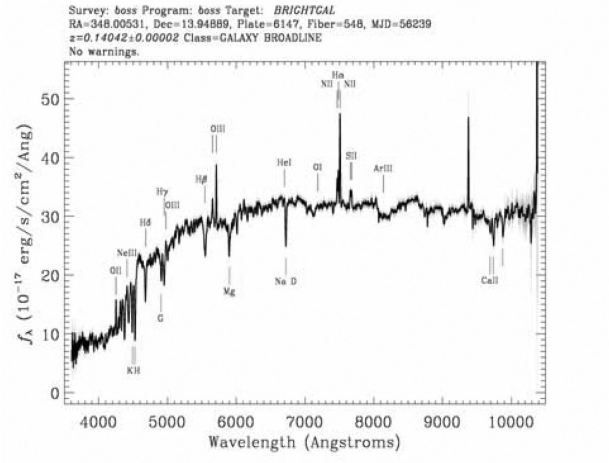

(e) **GRG19 spectrum**

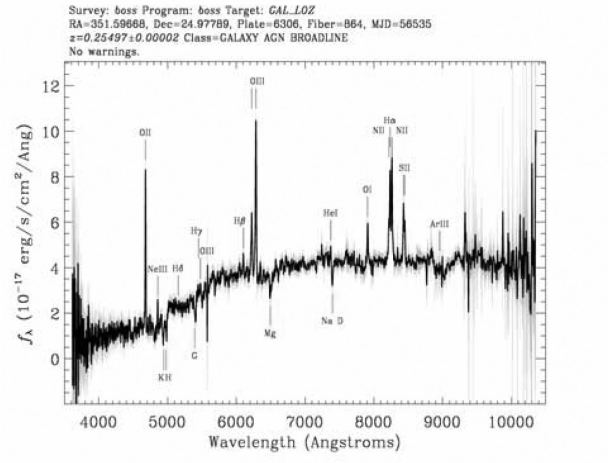

(f) **GRG21 spectrum**

Figure A1. Spectra of hosts of GRG1, GRG2, GRG7, GRG10, GRG19 and GRG21 obtained from the SDSS DR12 sky server.

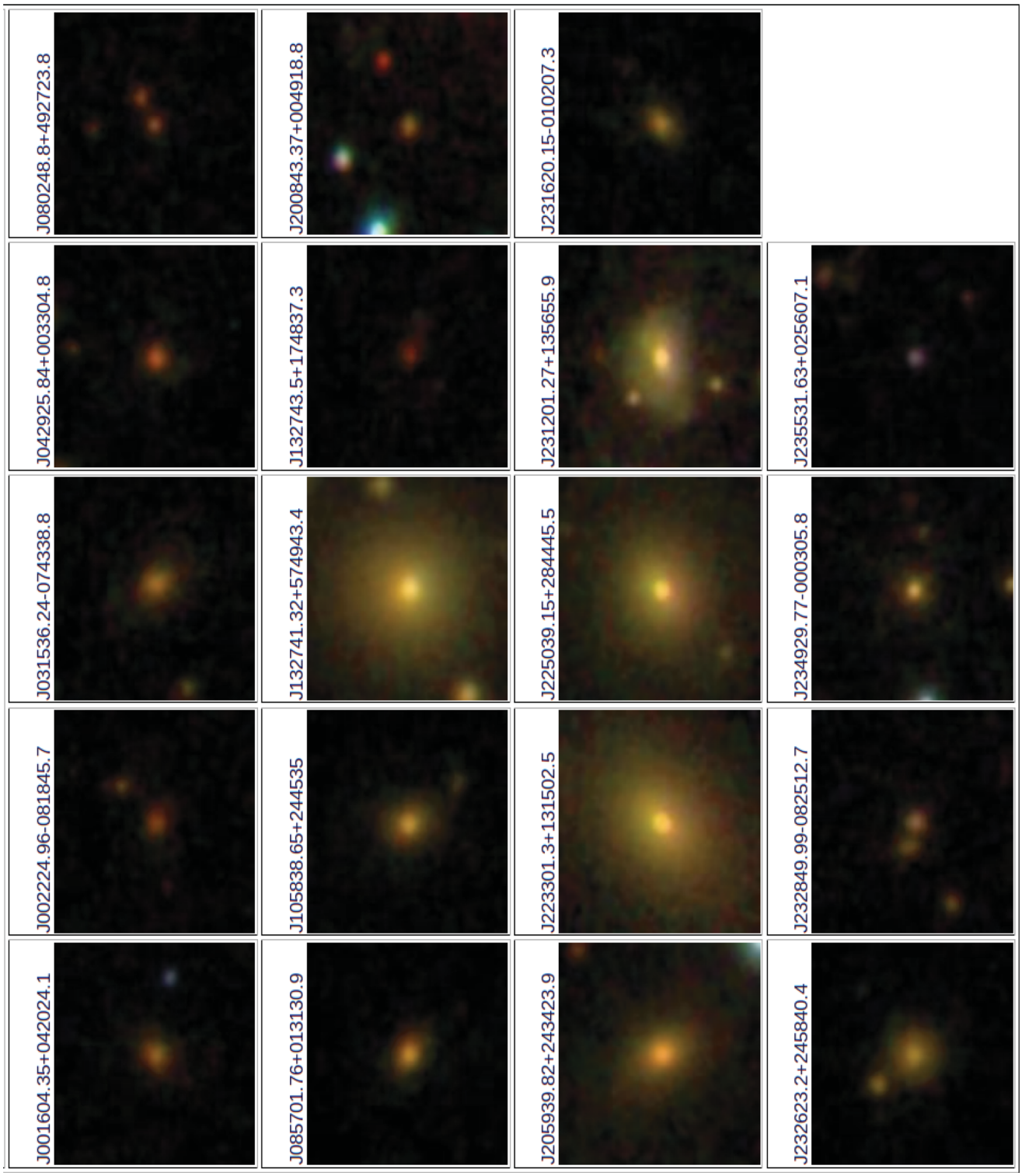

Figure A2. Optical images of host galaxies of GRGs from SDSS.

This paper has been typeset from a TEX/LATEX file prepared by the author.